Innovative, Low-Mass, Passively Cooled, All Composite Material Tower Structure for High Resolution Charged Particle Tracking in a Gamma-Ray Space Telescope

NASA SBIR #97-1 17.01-5179
Phase I Final Report

Eric Ponslet, Steve Ney, and William O. Miller
HYTEC Inc.
October 7, 1998

DESIGN ENGINEERING
ADVANCED COMPOSITE APPLICATIONS
ULTRA-STABLE PLATFORMS

110 EASTGATE DR., STE. 100
LOS ALAMOS, NM 87544

PHONE 505 661 3000
FAX 505 662 5179
WWW.HYTECINC.COM

1. Project Summary

The objective of this project is the development of ultra-lightweight support structures for high precision space-based instruments. The structures are intended to support sensitive instruments and must provide dimensionally stable supports for those detectors, incorporate efficient passive cooling technology to conduct dissipated heat away from the detectors, and be able to survive severe loads and vibrations during launch.

For particle tracking silicon detectors such as those used in the GLAST experiment (a NASA mission planned for launch early next century) HYTEC has introduced an innovative concept of building support structures by stacking trays on top of one-another and holding the stack in compression with tensioned Kevlar cables. This technology offers significant advantages of ease of assembly and testing and a potential for substantial improvements in containment angles for Gamma-Ray astronomy because of radical reductions in the amount of structural materials used.

The objectives of Phase I were to demonstrate the feasibility of the stacked tray concept, validate design and analysis approaches by comparing predictions of dynamic behavior with measurements, and experimentally evaluate a prototype assembly for its ability to survive random vibrations during launch.

During the Phase I period, a complete prototype was built and tested at HYTEC. The prototype is a stack of ten square trays, stacked to form a tower-like structure, and held together by four tensioned Kevlar cables running through the corners. Both detailed finite element and faster lumped parameter models were used to predict static and dynamic responses of the structure. Those predictions were compared to experimental data from a series of modal tests performed on the prototype trays and tower. The comparison showed extremely good analytical-experimental agreement, thereby validating the simulation techniques for use in advanced design development. Finally, the prototype tower was subjected to harsh random vibration qualification tests and survived without damage, confirming the feasibility of the stacked tray concept for use in space-based instruments.

With a design concept and the associated simulation techniques successfully validated in Phase I, the potential benefits from the stacked tray design clearly call for further development. In Phase II, the design will be optimized for minimum mass and maximum “transparency” to charged particles, as well as thermal conductivity. Those design goals make advanced composite materials a prime choice for the structural elements of the trays. Carbon-Carbon composites have very large radiation length, high thermal conductivity, and high stiffness and strength. The Phase II design will make use of this material, together with other advanced composites like resin based graphite fiber laminates and ultra-lightweight carbon honeycombs to provide a tray structure that aggressively minimizes mass and maximizes heat transport capacity. Phase II will culminate with the construction of a 17-tray stack that will be thoroughly tested for dynamic signature, thermal performance, and survivability to launch vibrations.

This innovative technology will produce support structures for sensitive space-based instruments with unprecedented levels of dimensional stability, heat removal capacity, and effective radiation length. The designs could find direct application in the GLAST experiment but also in other instruments (like optical platforms) requiring high dimensional stability, and in small, high thermal conductivity structures for passive cooling of opto-electronic systems and high-density electronic devices such as laptop computers.

Table of Contents

2. Summary of Phase I Goals, Achievements, and Main Conclusions

This phase I SBIR project was intended to demonstrate feasibility of a novel design concept for multi-layer, silicon strip detector based, gamma-ray telescope systems. The concept consists of stacking several panels (trays) carrying silicon detectors on top of each other in alternating directions to form a "tower". The panels are separated from each other by small corner bosses or spacers that contain alignment pins. The stack is held together by cables that run though the corners and the tubular alignment pins.

The primary goals of this phase I effort were:

- to demonstrate the mechanical feasibility of the stacked tray concept by fabricating a prototype tower. Areas of particular interest include cable selection and termination techniques, assembly and disassembly techniques and fixtures, and alignment of the assembled tower.
- to exercise and validate design and modeling techniques for these structures, and in particular verify the ability to predict the dynamic characteristics of trays and towers by comparing simulations with test data obtained on the prototype.
- to evaluate the design for its capacity to endure the vibrations associated with a space launch by subjecting the prototype to a typical random vibration qualification test for space launched equipment.
- to capitalize on the accumulated experience and data to critically review the design and propose improvements and/or changes for continued development in phase II.

During the course of this six month program, the goals outlined above were reached by fabricating a complete tower of 10 trays, demonstrating the validity of analytical predictions of dynamic behavior of the trays and tower, and successfully subjecting the tower to qualification tests without damage.

Some of the notable achievements are listed below:

- Detailed mechanical design of the trays and tower was completed and all components necessary for fabrication of 10 trays were acquired.
- various types and sizes of Kevlar cable were tested at Hytec to evaluate their pull strength. Various cable termination techniques were also developed and tested.
- Ten trays were fabricated at Hytec using a number of specially designed tools and fixtures. These trays were assembled into a complete tower.
- material characterization tests were performed to measure critical properties of materials used in the tray fabrication, such as graphite epoxy laminates and reticulated vitreous carbon foam.
- finite element models of single trays and entire towers were generated and used to predict static and dynamic response.
- single trays and the entire tower were tested to determine their modal characteristics and compare them to predictions; agreement was in general excellent.
- the complete tower successfully survived the random vibration qualification tests specified for space launched equipment. No detectable damage resulted from those tests.

Primary conclusions from the Phase I activities can be summarized as follows:

- the stacked tray concept, with synthetic cables entirely responsible for holding the stack together is a viable one; the prototype tower successfully endured random vibration qualification tests.
- the use of tubular centering pins and closely controlled dimensional tolerances on the tray corner pieces effectively produces a tower with small and predictable errors in tray to tray alignment. Fabrication and assembly of structural components did not reveal any problems.
- although the cables alone can be sufficiently strong to hold towers together, a substantial improvement in tower dynamics can be achieved by attaching full-coverage side-walls to the tower and relying on those walls not only for passive evacuation of waste heat but also as structural components. Using this approach, stiffness requirements for the trays themselves are lessened and the amount of structural material in the trays can be reduced, potentially leading to a lighter tower.
- finite element models of these concepts give very good analytical estimates of their behavior. These models can also effectively be used to adjust simpler lumped parameter dynamic models that can then be used to predict random vibration response and to quickly explore the effects of various design parameters.
- testing samples of any unusual or advanced material to be used in the design is critical to guarantee predictability via analysis. Data obtained from vendors are not reliable because of variations in manufacturing parameters.
- correlations between test data and analytical predictions of tray and tower dynamic response proved excellent once material properties were accurately identified.

3. Mechanical Design of Prototype Trays and Tower

3.1 Description of Design Concept

The concept is for a mechanical support structure for particle tracking detectors using multiple layers of silicon-strip detector chips. The structure (Fig. 1) consists of a stack of identical “trays”, sitting on top of one-another on small corner posts, and held in compression by four synthetic braided cables running thought the corners and pre-tensioned.

Each tray has a grid of silicon strip detector chips bonded on each side. The strips run in the same direction on both sides. A tower is built by stacking several trays and clocking each tray 90 degrees relative to the previous one, thereby creating a 3 dimensional tracking matrix for charged particles. The tray structure used in Phase I is shown in Fig. 2; it is typical of a tray configuration planned for the GLAST gamma-ray telescope. The tray is essentially a thick, lightweight sandwich panel with a core, two face sheets, and a closeout frame. The face sheets carry a payload of lead converter pieces, flexible printed kapton bias circuit, and silicon detector chips. In GLAST, biasing and pre-conditioning electronics for the detector chips are concentrated on circuit boards mounted on two opposite sides of the trays (not shown in Fig. 2).

The trays are stacked on top of each other with small spacer blocks establishing the proper spacing at their corners (Fig. 3). Note that the spacers would normally be a single piece with the tray closeout frame; separate blocks were used in Phase I for ease of fabrication. Precision holes are drilled in the corners of the closeouts and through the spacer block to receive

tubular alignment pins and tensioning cables that run through those pins from bottom to top of the tower.

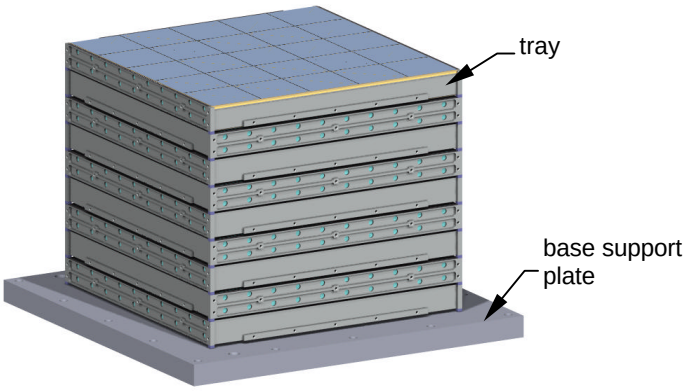

Figure 1: a 10-tray silicon strip detector based particle tracking tower.

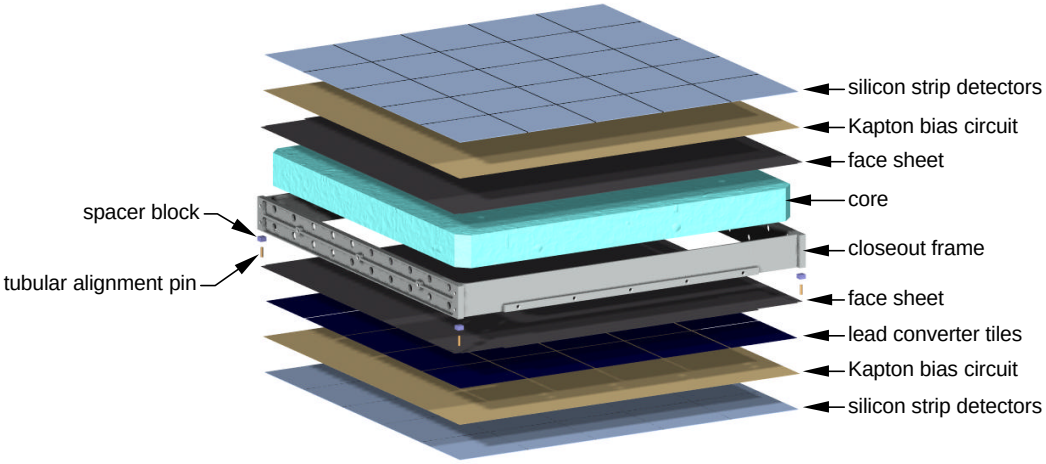

Figure 2: exploded view of a prototype tray with realistic payload (type A).

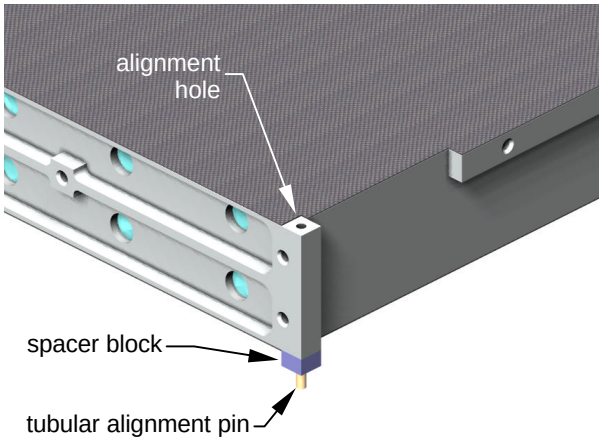

Figure 3: close-up view of the corner of a tray, with corner spacer block and tubular alignment pin.

In GLAST, side-walls must be attached to the sides of the tower to provide an efficient thermal path to conduct waste heat from the electronics away from the detectors. Those walls are not shown in Fig. 1. Note that the initial motivation for the walls is purely thermal. The objective of Phase I was to demonstrate the structural integrity of a stacked tray concept without depending on the additional shear stiffness than can be obtained form the side-walls. For that reason, the prototype designed and built in phase I and shown in Fig. 1 does not contain the 4 side-walls.

However, using the side-walls not only as a thermal design component but also as a primary structural member is a tempting option. For that reason, and to demonstrate any structural advantage of that solution, tests were performed both without and with side-walls to establish the structural characteristics of both configurations.

3.2 Mechanical Design Requirements and Design Approach

As mentioned above, ***the phase I tower is designed without side-walls***. In phase I, trays and tower are designed based primarily on pseudo-static load factors typically used for preliminary design of space launched equipment. Thermal, vacuum, and acoustic coupling issues are not considered (thermal issues will be addressed in phase II). Also, dynamic stresses due to random vibration are not analyzed in detail or considered explicitly in the design phase; however the tools necessary for such calculations are established and validated by testing so that they can be used reliably in design calculations for phase II hardware.

With this in mind, the structures were designed for static load factors between $-2g$ (traction) and $+10g$ (compression) in the launch (Z) direction, and between $+4g$ and $-4g$ in any transverse direction (XY plane). One g is equal to the standard acceleration of gravity, or 9.81 m/s^2. Nowhere in this phase I design was particular attention devoted to really minimizing mass; *the design is a proof of concept and predictability of behavior is the primary concern*. Minimum weight designs will be developed in Phase II.

Critical design aspects include:

- the amount of tension in the corner cables required to hold the trays tightly stacked together as well as a technique to hold the ends of the cables under such preload
- the level of compressive stress induced in the spacer blocks and the corners of the tray closeouts by the cable tension combined with the applied accelerations
- the static and dynamic deflections of the trays (largest at the center) must remain small to avoid contact between successive trays, and destruction of detector chips and wire bonds.
- although not an issue for an isolated tower, in multi-tower designs like GLAST the tower deflections must remain small to avoid contact between neighboring towers.

The following sections summarize design calculations and simulation results that were performed to address those issues. The actual design process was of course heavily iterative; only final calculations are presented in this report.

The design calculations were based on a 17-tray tower, the current baseline configuration for GLAST. Note however that, both to limit expenses and fabrication time, the prototype tower built in phase I only has 10 trays. This of course provides additional safety margins and will have to be accounted for when extrapolating the lessons learned in testing the prototype to a taller, 17 tray tower.

3.3 Cable Tension and Corner Stresses

3.3.1 Design Calculations for 17-Tray Tower

Since the tower is designed without sidewalls, the corner cables are entirely responsible for keeping the tower together. As explained above, the design load factors are +10*g*/-2*g* in the launch direction and +/- 4*g* in the transverse plane. This section describes calculations of the required level of pre-tensioning in the cables to insure tower integrity during launch. Corner stresses are also evaluated.

A primary assumption in the following calculations is that the spring constant of a corner cable is substantially smaller than that of the corner itself (i.e. the stack of 17 corners of the aluminum closeout frames and the 18 spacer blocks). This allows one to treat the cable tension as a constant, not affected by launch strains in the aluminum parts. Note that this assumption is clearly satisfied when using synthetic braided cables which were found to stretch by about 6 mm when tensioned during tower assembly.

Also, because an actual flight-like tower would have its bottom tray completely anchored all around the edges to the supporting base structure, the lowest interface considered in these calculations design is between trays 1 and 2. Note that in actuality, and for reasons of simplicity, the prototype was built with a bottom tray identical to all others and supported on the base plate via 4 spacer blocks (visible in Fig. 15, right).

The role of the cables is to maintain sufficient contact pressure at every tray-spacer block interface such that:

- these interfaces never completely unload and open during launch
- the worst case (lowest) residual pressure on the interfaces is sufficient to prevent transverse slippage under the worst case (highest) lateral loads (we did not want to rely on the tubular pins to contribute lateral strength).

Minimum cable tension to avoid slippage:

The worst case situation for slippage occurs when external loading conditions combine to reduce the vertical loads on a particular corner block to the lowest value while at the same time exerting the largest transverse loads on that interface. Note that this is actually unlikely to occur during launch because maximum transverse accelerations do not typically occur at the same time as maximum longitudinal accelerations.

The worst case (largest) lateral interfacial loads occur at the bottom of the stack (interface between trays 1 and 2), when the 16 trays above it are pushed in the transverse direction with a 4*g* load factor. Assuming no slippage, the corresponding transverse load max(F_t) on each corner block is

$$\max(F_t) = \frac{16M\,4g}{4} = 16Mg = 157 \text{ N}, \qquad (1)$$

where M is the mass of one tray (1 kg), and g is the acceleration of gravity (9.81 m/s^2).

The worst case (i.e. lowest in this case) pressure on that interface occurs when the pressure exerted by the cables is reduced by the –2*g* vertical acceleration combined with the reaction to the overturning moment due to the 4*g* lateral acceleration which further unloads 2 of the 4 corners. The residual pressure min(F_n) on the 2 lightest loaded corners is then given by

$$\min(F_n) = T - \frac{16M2g}{4} - \frac{16M4gh}{2b} = T - 8Mg - 32\frac{Mgh}{b} = T - 319.2 \text{ N}, \quad (2)$$

where h is the vertical distance from the interface to the center of mass of the 16 trays above (0.253m), b is the corner to corner dimension of the tray (approximately 330 mm), and T is the tension preload in each corner cable.

To prevent slippage, the ratio of max(F_t) to min(F_n) must be less than the expected coefficient of friction for an aluminum-aluminum interface, i.e.

$$\frac{\max(F_t)}{\min(F_n)} < \alpha_{Al-Al}, \quad (3)$$

where $\alpha_{Al\text{-}Al}$ is the static coefficient of dry friction for an aluminum on aluminum interface (i.e.$\alpha_{Al/Al}$=1.05 [1]). Solving (1), (2), and (3) for T we get

$$T > 469 \text{ N}. \quad (4)$$

Minimum cable tension to avoid separation:

To avoid separation at the lowest interface, the residual compression at that interface must remain positive at all times. The worst case occurs again if the –2g vertical acceleration combines with the overturning moment from the 4g lateral acceleration, reducing the compressive force on 2 of 4 corners. To maintain contact we must have:

$$\min(F_n) = T - \frac{16M2g}{4} - \frac{16M4gh}{2b} = T - 319.2 \text{ N} > 0. \quad (5)$$

Solving for T, this leads to

$$T > 319 \text{ N}. \quad (6)$$

Design value of cable tension

From conditions (4) and (6), and imposing a safety factor of 2 (100% safety margin) because of the catastrophic nature of a cable or corner post failure, we settle on a tension in each cable at the time of assembly of

$$T = 944\text{N} \ (212 \text{ lbf}). \quad (7)$$

The safety factor for separation is then approximately 3 (200% margin). Note that because some amount of relaxation must be expected in synthetic cables, the assembly procedure for the tower includes keeping the cables under constant tension for a few hours before attaching the cable terminations. This eliminates the largest portion of the relaxation.

Corner Stresses

An approximation of the compressive stress in the corner blocks can be obtained by superimposing simple beam solutions for local bending stresses and direct calculations of worst case compressive stresses.

The worst case static compressive force max(F_n) on a corner piece occurs when the cable tension T is augmented with 10g vertical acceleration and the overloading from the overturning moment at 4g transverse acceleration. It is given by

$$\max(F_n) = T + \frac{16M10g}{4} + \frac{16M4gh}{2b} = 1569 \text{ N}, \quad (8)$$

and is distributed across the cross section of a corner block, c^2, where c is the lateral dimension of the corner block (5.5mm). The resulting direct compressive stress is

$$\max(\sigma_c) = \frac{1569}{c^2} = 52 \text{ MPa.} \quad (9)$$

In addition, a bending moment M_b is induced in the corner blocks by transverse accelerations. This bending induces an added distribution of normal stresses, σ_b. The largest bending moment, evaluated at the contact plane between the corner block and the tray above is roughly equal to

$$M_b = \frac{1}{2}\frac{16M}{4}\frac{4gd}{4} = 0.314 \text{ Nm,} \quad (10)$$

where d is the height of a corner block (4 mm) and the factor ½ accounts for the fact that, as long as contact is maintained, the shear imposed on the corner block is balanced by equal bending at the top and bottom contact surfaces of the corner block. This gives a maximum bending stress at the edge of the block of

$$\max(\sigma_b) = \frac{\max(M_b)c}{2I} = \frac{6\max(M_b)}{c^3} = 11 \text{ MPa.} \quad (11)$$

Adding the direct normal stress and the bending stress we get an expected maximum normal stress in the block of about

$$\max(\sigma_n) = \max(\sigma_c) + \max(\sigma_b) = 63 \text{ MPa.} \quad (12)$$

For 6061-T6 (see detailed tray design, Section 3.5), the yield strength is about 255 MPa, giving us a safety factor of 4.

3.3.2 Expected Levels for 10-Tray Prototype

The 10 tray prototype was assembled with the same cable preload as calculated above. This provides a realistic test of cable strength and termination techniques. However, because of the reduced height of the tower and the lower total mass, the coefficients of safety against slippage and separation are increased and the corner stresses decreased from their expected values in the 17 tray tower.

The new values can be obtained following the same reasoning as above, this time considering the reactions from 9 trays (instead of 16) on the lower tray interface; the new value for h is 144 mm.

Safety against slippage: factor 3.4, 240% margin
Safety against separation: factor 4.8, 380% margin
Safety against yield: factor 5.4, 540% margin

Note that, consistent with the static design approach used in Phase I, dynamic amplification was not considered in these calculations; the large safety factor is providing some margin for dynamic effects.

3.4 Tension Cable Design and Testing

The stack of trays is held together by 4 cables, running through the corners and pre-tensioned at assembly. The material used for these cables would ideally have very high strength,

high elongation to failure (so the amount of tension is more easily controllable), low density, and high radiation length (*RL*).

Braided cables made of Kevlar 29 are ideal candidates†. Kevlar 29 fibers are among the toughest synthetic fibers in existence, their density is very low, they have a high elongation to failure, and likely a high *RL* (a published value could not be found). Table 1 lists typical properties.

property	typical value
density	1.44 g/cm^3
fiber diameter	12 μm
elongation to failure	4%
elongation modulus	70 to 100 GPa
ultimate stress	3100 MPa

Table 1: typical properties of Kevlar 29 fibers[2].

Braided and twisted cables are readily available from various manufacturers and they have been used in space applications.

3.4.1 Cable Selection

The design calculations of Section 3.2 call for a cable with an ultimate strength largely in excess of 210 lbf. A number of samples of various size cables were obtained from a few vendors and simple static pull strength tests were performed to evaluate them. The results are listed in Table 2.

		Break Strength (lbf)	
cable type (OD in inches)	**Manufacturer**	**Listed**	**Measured**
Model aircraft control line, braided (0.026)	unknown	200	85
Plastic sleeved twisted strands (0.045)	Phillystran	350	318
Bare twisted strands, 1-6 wrap (0.065)	Phillystran	700	400
Braided 8x1000 (0.047)	Cortland	300	304
Braided 6x1500 (0.053)	Cortland	325	286
Braided 12x1500 (0.065)	Cortland	800	not tested

Table 2: measured breaking strength of Kevlar cables of various dimensions and from different sources.

Braided design from Cortland Cable[3] showed good loading response and overall strength; the measured break strengths were consistent with specifications from the vendor. Also, the braided design is easier to work with than twisted strand designs.

Since breaking even one of the corner cables would result in catastrophic failure of the tower, we selected a 12 x 1500 braided Kevlar cable (.065" outside diameter). This cable is rated at 800 lbf (3560 N) ultimate strength, leading to a safety factor of almost 4 over the design value for cable tension. Clearly, the critical elements are termination techniques that can hold the required load. This is addressed in the next section.

3.4.2 Termination Technique

Terminations are always the critical aspect of the design of a cable. The termination must be able to sustain whatever load the cable assembly is designed for without slipping, while stress

† Kevlar fibers are widely available in two grades: Kevlar 29 is a low modulus grade, while Kevlar 49 has a higher modulus (about 40% higher), and a lower elongation to failure, for about the same ultimate stress.

concentrations make the cable weaker near the terminations. Several approaches were considered but quickly reduced to the use of small diameter swaged and/or potted terminations because of limited available space. A number of variations were tested for pull strength (see Fig. 4 and Table 3).

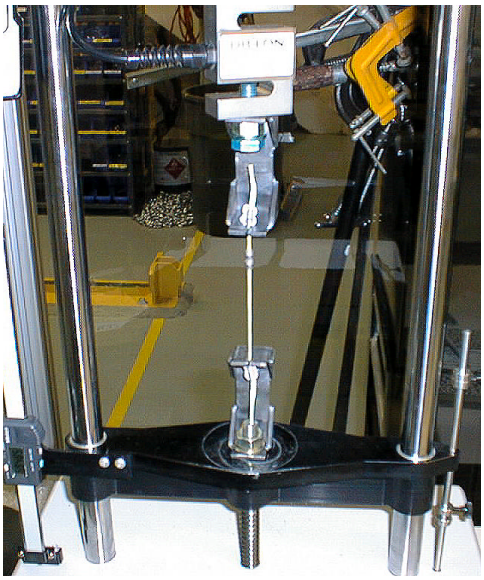

Figure 4: measuring holding strength of cable termination techniques.

cable type	termination type	ultimate load (lbf)	failure mode
Cortland 8x1000	brass tube (5/64" OD), potted with CyA resin.	90	brass tube sheared
Cortland 8x1000	brass cylinder (1/4" OD), potted with CyA resin	80	bond between CyA and brass
Cortland 8x1000	swaged copper sleeve (1/32" wall)	80	sleeve slips on cable
Cortland 8x1000	swaged copper sleeve (1/32" wall) + CyA potting	145	Kevlar cable brakes at edge of sleeve
Cortland 6x1500	two swaged copper sleeves (1/32" wall) + CyA potting of outer sleeve	200 to 260	Kevlar cable breaks at edge of inner swaged sleeve
Cortland 12x1500	two swaged aluminum sleeves (?? wall) + CyA potting of outer sleeve	350 to 360	Kevlar cable breaks at edge of inner swaged sleeve

Table 3: holding strength for various termination techniques used on Kevlar cable.

The best results were obtained with a double swaged aluminum sleeve, combined with potting of the fibers in the outermost sleeve, using a fast cyano-acrylate adhesive. Interestingly, we found that potting the fibers in both swaged pieces instead of just the outer one lead to much weaker cables: this is likely explained by the stiffening of the cable in the transition region that causes an even sharper stress concentration. For those terminations that are made with the cable under tension (like those at the top of the tower), better results were obtained with a small piece

of tubing or rod inserted in the cable immediately next to the outer swage piece. This spreads the cable strands apart and allows better penetration of the cyano-acrylate (see Fig. 5).

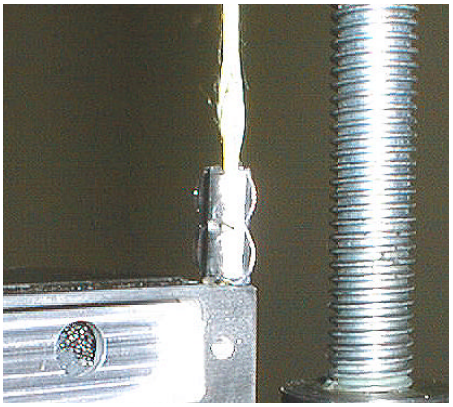

Figure 5: the most successful termination technique uses two aluminum sleeves, swaged on the cable, with the fibers potted in the outermost (top) sleeve with cyano-acrylate resin.

3.5 Detailed Design of Prototype Trays

The design dimensions, in particular wall thicknesses in the closeout frame, the dimensions of the corner blocks, and the thickness of the face sheets, were settled based on iterations of hand calculations of cable tension and corner stresses, FE models of trays, and a simplified FE model of a full tower (with the lower 3 trays modeled and the rest of the tower represented by a concentrated mass & inertia).

The closeout is a single piece of aluminum alloy (6061-T6), machined to shape (Fig. 6). Aluminum alloy was selected for this prototype because it is widely available, low cost, easy to machine, and relatively high strength (6061-T6). Aluminum is of course not a likely choice for a final design: materials with longer radiation length are preferable (fiber reinforced resin matrix composites, or carbon matrix composites, for example).

The closeout is essentially a square frame, about 28 mm thick by 330 mm on a side, with a wall thickness of 2 mm all around. Two opposite sides have a 4 mm thick bosses intended for heat removal from preamplifier circuits. Those bosses also provide additional stiffness and bonding area for the face sheets. The other two sides of the tray are stiffened by 3 ribs, 3.8 mm deep, running the whole length of those sides. The outer ribs (1 mm thick) also serve as bonding surfaces for the face sheets. The center rib is 2 mm thick and also has carries 3 threaded holes for attaching optional side-walls

At each corner, the closeout includes a corner piece consisting of a 5.5 by 7 mm column with a precision drilled hole for the alignment pins and tensioning cable. The corner piece is the primary load path providing stiffness to the stack. The 3 ribs on two of the 4 sides rigidly connect the corner piece to the rest of the tray (and transfer transverse loads into the face sheets).

A number of threaded holes (for #2 screws) are drilled in the corner pieces, ribs, and bosses to allow attachment of optional side-walls.

The rest of the tray structure is a thick sandwich plate, with nominally 300 micron thick face sheets separated by a 28 mm thick lightweight core. The core, closeout, and face sheets are joined by bonding with room temperature epoxy adhesives.

In a final design, candidate materials for the core must have high shear modulus, low mass, high *RL*, and low outgassing (in-vacuum or in-space instruments). Foams (aluminum, beryllium, carbon) and vented honeycombs (aluminum, graphite) have these characteristics. Foams are available with volume fractions as small as 3%, while commercially available aluminum honeycombs can reach about 0.6%, with comparable shear moduli. One concern with honeycomb is its non-homogeneous nature which leads to localized, non-uniform multiple scattering of charged particles and results in loss of performance for a gamma-ray telescope like GLAST. Note that this issue was recently examined by the GLAST project; the tentative conclusion is that honeycomb with walls up to 1 or 2 thousands of an inch (25 to 50 microns) will not present a problem for GLAST's Gamma-ray astronomy.

For the prototype trays built in Phase I, the primary selection criterion was immediate availability and ease of use (most fabrication operations were performed in-house, with minimal equipment). Our only option was to use a reticulated vitreous carbon (RVC) foam, with 3% volume fraction and 60 pores per inch (metal foams and honeycombs were not available within the Phase I timeframe). This foam has the advantage of being extremely easy to cut and shave to size (with sandpaper). This feature made assembly of the trays much easier without specialized machinery (metal foams or honeycombs must be machined to size with mills). However, we would not recommend the use of carbon foam in the final design of trays for an instrument like GLAST, primarily because of the lack of toughness of those foams and the inevitable release of small conductive carbon particles. Note that various treatments (light densification by vapor deposition, coating with diluted polymers, etc.) might be considered to improve the behavior of carbon foam and make it a viable candidate.

Materials to consider for the face sheets must have high modulus, low density and high *RL*. Graphite fiber/resin systems are ideal candidates: they have extremely high modulus, high *RL* (second only to Beryllium), are not easily damaged in handling, can be made into very thin plates and have excellent bonding strength with structural epoxies. Carbon matrix composites are a better choice if through-the-thickness thermal conductivity is required (this will be looked at in Phase II). In this Phase I study, we selected a readily available quasi-isotropic layup of 6 plies of unidirectional pre-impregnated tape. The plates are nominally 300 microns thick. The tape has XN50 graphite fibers (2K tows) in an epoxy matrix. Because of their high cost, these composite face sheets were used on only 3 of the 10 trays (referred to as *type A* trays); the remaining trays received aluminum alloy face sheets (*type B* trays).

4. Fabrication of Prototype Trays and Tower

4.1 Procurement and Preparation of Components

Most components necessary for fabrication of the trays were purchased from and/or prepared by specialized vendors and local machine shops. This includes closeout frame, face sheets, core material, engineering grade silicon chips, and dummy aluminum tiles. The lead converter tiles were provided by Bruce Feerick of the Stanford Linear Accelerator Center (SLAC). Some components required finishing operations that were performed at HYTEC (kapton bias circuits, foam cores). The following sections provide more details on those parts.

4.1.1 Aluminum Closeout Frames

These frames (Fig. 6) were machined from 6061-T6 aluminum alloy plate stock. The external features (ribs, heat transfer bosses, corners with holes, tapped holes) were CNC machined before removing the centers. Tight tolerances were imposed on the location of the holes for tubular pins and cables because they eventually define the tray to tray centering accuracy, and on the height of the corner posts which define the straightness of the assembled tower. The centers were then removed via wire EDM operations.

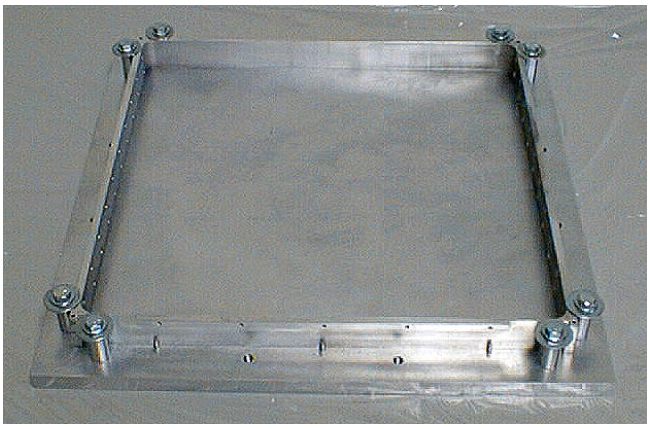

Figure 6: finished aluminum tray closeout frame (shown held in part of a bonding fixture that prevents deforming the very thin piece).

We were initially concerned that the frames would significantly deform after removal of the centers because of residual stresses in the material and/or stresses induced by the machining operations. This did not occur for a number of reasons. Plate stock is actually stress relieved at the mill so the level of residual stresses is low. Great care was taken during machining. Finally, wire EDM cutting is a very gentle technique: the part to be cut is submerged in a bath of electrolyte at room temperature during the cut, maintaining a very constant and uniform temperature in the metal. The wire cuts by electrically eroding material, without actual contact with the part. A finished frame is shown in Fig. 6, held in a protective fixture. Dimensional measurements on the finished frames revealed a small amount of bow in the sides of the frame, never exceeding 120 μm. The bow can be later recovered by careful fixturing during bonding of the face sheets and core.

An important note is that miscommunication with the machine shops lead them to knock off all sharp corners on the finished closeouts, including the critical corner pieces. This results in a substantial reduction in contact area with the spacer blocks (which underwent the same treatment), and a corresponding loss of stiffness and increase in stress levels. Close examination of the finished pieces indicates that up to 1mm of the 5.5x5.5 m lands are lost due to this chamfering. The models used for response predictions (see Section 6) were modified to approximate this effect.

4.1.2 Foam Cores

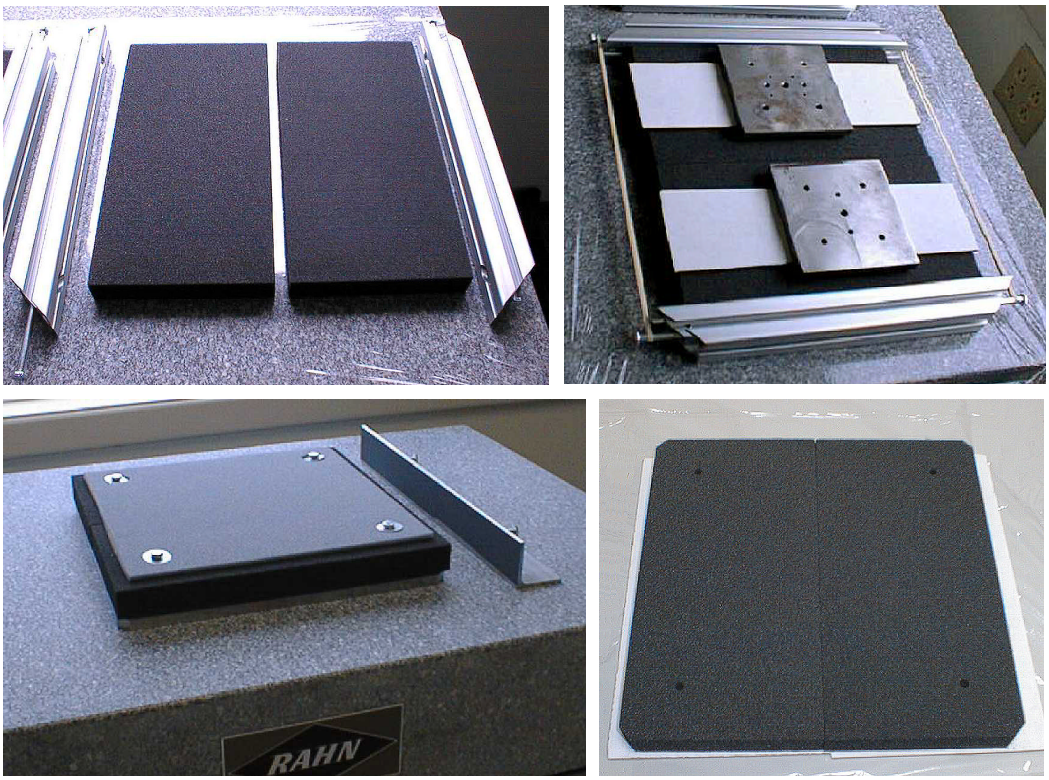

Figure 7: core preparation process: two halves are prepared and bonded together (top), then the edges are shaved (bottom, left) to achieve exact lateral dimensions to fit the closeout frame (bottom, right).

The cores were purchased rough cut to oversized dimensions. For availability reasons, 2 pieces had to be bonded together to form each core block (Fig. 7, top). After bonding, the cores were shaved to exact lateral dimensions using a steel template and right angle sanding block (Fig. 7, bottom). The finished core blocks fit exactly inside the frames with a .004" radial clearance for the adhesive. At this point the thickness of the core is still about .040" more than that of the frame; this is shaved off during assembly of the tray (see section 4.2.1).

4.1.3 Carbon Face Sheets

The sheets were laminated and cured by an outside vendor and later cut to size (with a contour matching that of the frame) with a water-jet cutting machine. The finished sheets have about 60% fiber volume fraction, a thickness of 318 μm, and an expected Young's modulus of about 100 GPa (15 million psi). See Section 6.1 for details on the mechanical properties. One side has a smooth finish where it was molded against the base platen, while the other has a rough finish due to the use of a textile bleeder ply. The rough side was bonded to the tray frame-core assembly since it is expected to give the strongest bonds.

As mentioned earlier, and to limit costs, only 3 of the 10 trays were assembled with graphite epoxy face sheets; the other 7 received aluminum alloy face sheets (6061-T6), 310μm (.012") thick. The membrane stiffness of these sheets is about 30% lower than that of their graphite/epoxy counterparts. Their mass is about 40% larger.

4.1.4 Bias Circuits, Converter Tiles, and Silicon Chips

Lead converter tiles (200 μm thick) were obtained from SLAC. These tiles are cut to size by milling a thick stack of lead sheets pressed between thick aluminum plates.

Because actual bias circuits were not available, we used raw kapton sheets of roughly the same total thickness. The sheets were cut to size in house.

Engineering grade silicon chips (400 μm thick) were used instead of actual detectors. No attempt was made to produce or simulate wire bonds.

4.1.5 Aluminum Payload Dummies

To save cost and complexity, 7 of the 10 trays did not receive lead, kapton, or silicon; aluminum tiles were used instead to approximate the mass loading. Thicker pieces are used on the bottom than on the top to simulate the mass of the lead converters.

4.1.6 Adhesives

All bonding was performed using two component room temperature epoxies from 3M's Scotchweld series[4]. These epoxies are available in dual syringe applicators, making dispensing and mixing convenient for prototype fabrication. Two types were used in the tray assemblies: DP190 gray, a slower, higher viscosity flexible epoxy, and DP125 translucent, a faster cure, lower viscosity and translucent epoxy.

DP190 was used to bond the structural sandwich together and the lead converter tiles. Its advantages are a higher viscosity and light gray color, allowing good control of the amount of adhesive used. A specially made plastic grooved wiper tool was used to control the amount of adhesive to a uniform layer, 100μm (.004") thick.

The lead converter pieces were sprayed with a water-based epoxy primer (Cytec, BR 6747-1[5]) prior to bonding. The primer is advertized to improve bonding strength and is used here to alleviate some of the difficulties related to bonding oxidized lead.

The faster DP125 was used in all subsequent operations, mainly to accelerate the production of the trays (pot life is 25 minutes for DP125, compared to 90 minutes for DP190). The translucent epoxy also made visual alignment of the arrays of silicon tiles or dummies possible, while the lower viscosity (15,000 cps compared to 80,000 for DP190) simplified the bonding of the large Kapton sheets (excess epoxy was easily rolled out to the edges and removed).

4.1.7 Spacer Blocks and Centering Pins

The spacer blocks provide the mechanical interface from one tray to the next and define the spacing between trays and overall straightness of the tower. They also receive the tubular centering pins.

The blocs are almost cubical pieces of 6061-T6 aluminum alloy, 5.5×5.5×4 mm, with a center hole for the pin. The height (4 mm) of the blocs is machined to a tight tolerance to insure accurate spacing from one detector layer to the next and guarantee the straightness of the finished tower.

The tubular pins were made with short sections of off-the-shelf miniature brass tubing (3/32" OD by .006" wall). These pins are not intended to be load carrying components of the tower (friction between trays and spacer blocks carries the loads); they provide lateral centering from one tray to the next and can also be used as reference features for positioning detectors on both face during assembly.

As mentioned in the closeout description, the spacer blocks were mistakenly machined with chamfered instead of sharp corners. The ensuing reduction in contact area affects both the stiffness of the tower and the stress levels. Models used for predictions (Section 6) account for this reduction.

4.2 Tray Fabrication

4.2.1 Structural Sandwich Fabrication

The first step consists of bonding *one* face sheet and the core block to the aluminum closeout frame (Fig. 8). Because the frame is very flexible, the bonding operation is performed in a fixture. The fixture consists of a ½" thick aluminum tooling plate (lapped to .003" flatness) with 4 precision drilled holes for corner pins that maintain the corner holes of the closeout frame in their exact location, and 12 more pins (3 per side) that prevent the sides from bowing out. The frame is pressed down on the face sheet with 16 clamps (only 8 shown in the picture). The core is pressed down on the face sheet by dead weights (~ 60 lb) distributed on top of it, and the entire setup is sitting flat on a precision marble block to prevent twisting.

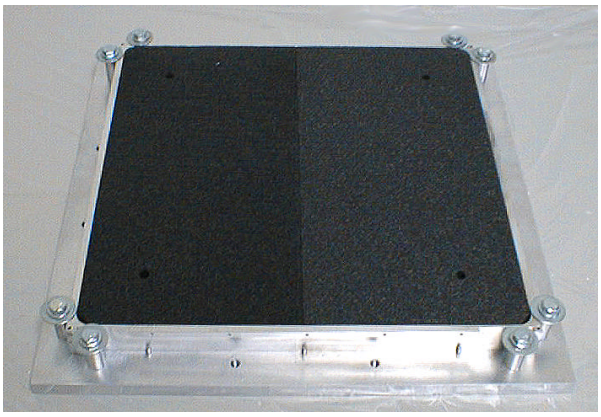

Figure 8: RVC foam core bonded to one face sheet (not visible in photograph) and the closeout frame; the next operation is to shave the exposed face of the core to match the thickness defined by the closeout frame.

After curing (24 hours at RT), the core is shaved to match the thickness of the frame (Fig. 9). This is done by carefully sanding the free face of the assembly on a large sheet of fine-grained sandpaper that has been bonded to the marble block.

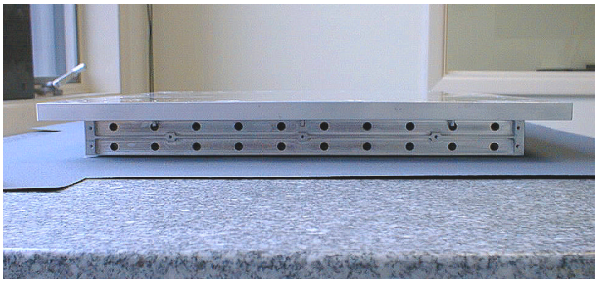

Figure 9: RVC foam core being shaved to exact thickness after being bonded to tray closeout frame and one face sheet.

Once the core has been shaved down to exact dimension, the second face sheet is bonded in place. The tray is again held in the fixture, this time mainly to prevent warping. Vacuum bagging is used to provide pressure on the face sheet during curing.

4.2.2 Payload (type A) and Dummies (type B)

Once the structural sandwich is complete, it is ready to receive its payload. The three carbon-faced trays receive a realistic payload of lead converter tiles (bottom side only), kapton sheets and silicon chips (both side). The various layers of the payload were bonded one at a time with epoxy adhesive (DP190 for lead on face sheet, DP125 for everything else). Vacuum bagging was used at every step to provide pressure during curing (see Fig. 10, left)

A tape transfer technique was used to achieve the regular tile pattern of lead squares and silicon chips. The pieces are first layed down on a printed mylar reference pattern that has been sprayed with a low-tack adhesive. The whole array of 25 pieces is then covered with a sheet of single sided, transparent, high-tack adhesive film (the transfer tape). That film is then pulled off the mylar pattern - carrying the pieces with it – and positioned on the tray, which has been spread with epoxy. The assembly is vacuum bagged and cured before the transfer tape is removed.

Note that bonding lead can be a difficult operation because of the oxide layer that is almost always present at the surface of the lead. A primer was used to help with this problem. Both sides of every piece of lead converter were sprayed with the primer (see Section 4.1.6).

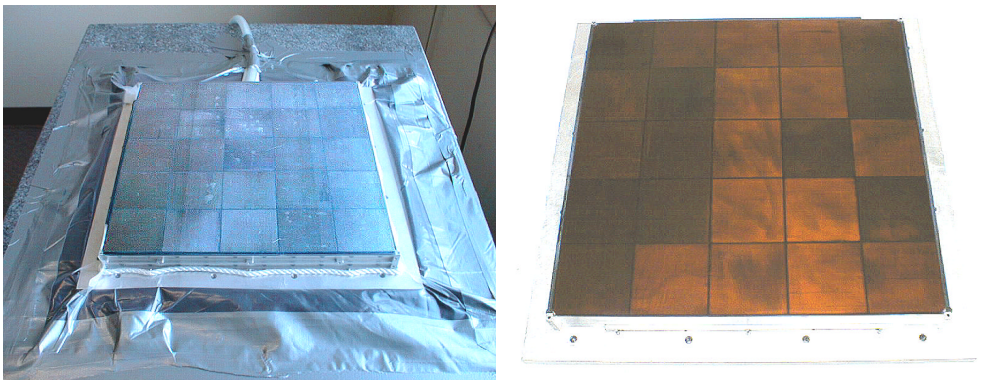

Figure 10: left: lead converter tiles being bonded to a tray with epoxy; vacuum bagging was used to apply pressure during most bonding operations. Right: tray with lead converter tiles and kapton layer in place.

Once all layers of the payload have been bonded to a tray, it is carefully cleaned to remove any excess epoxy (during bonding of the payload, excess epoxy tends to be pulled out by the vacuum bagging), and clear the pin holes and threaded screw holes. Finished trays are shown in Figs. 11 and 12.

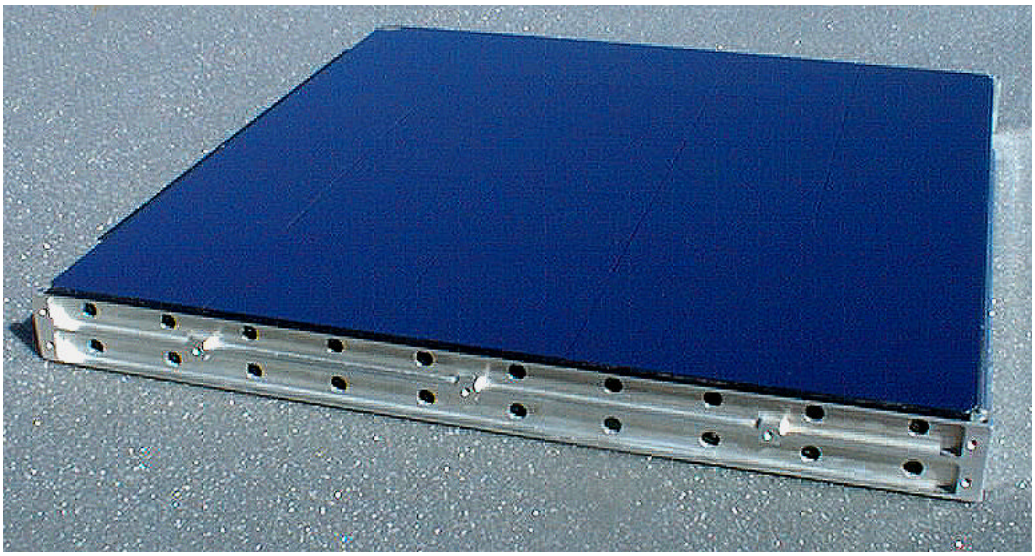

Figure 11: finished type A tray with graphite face sheets, lead, kapton, and silicon in place.

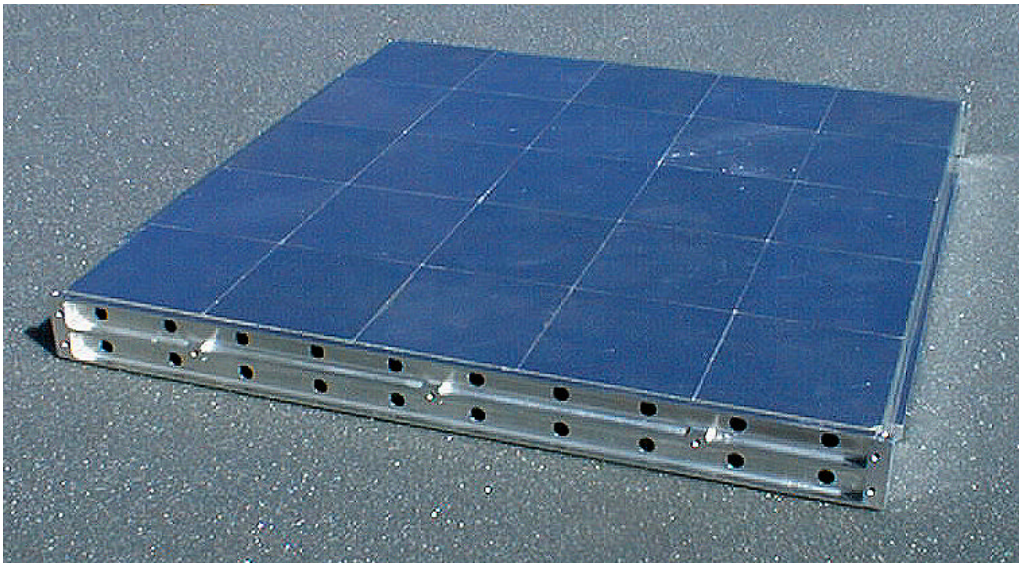

Figure 12: finished type B tray with aluminum face sheets and aluminum dummy tiles to simulate payload.

4.3 Tower Assembly

The stacking sequence for assembling a complete tower requires alternating layers of tray and spacer blocks with tubular pins, threading the Kevlar tension cables through the corners, tensioning those cables to the prescribed load, and swaging cable terminations to maintain that preload.

The tower was assembled as shown in Fig. 13. The more realistic type A trays were used at the lower 2 levels, where the largest stresses and high frequency vibrations are expected, and at the top of the tower, where the largest low frequency accelerations are expected.

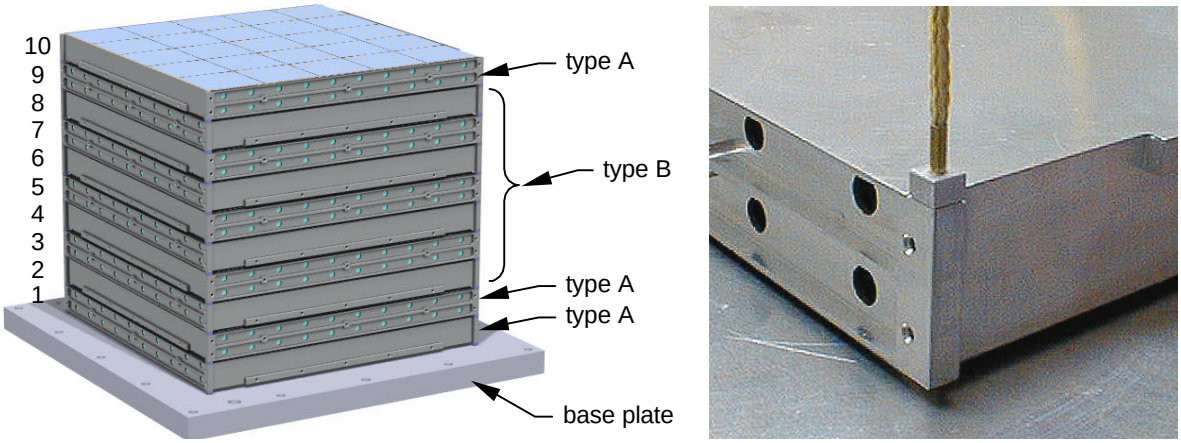

Figure 13: stack configuration used in the 10-tray prototype tower (left) and detail of corner spacer block, tubular pin and Kevlar cable (right).

The entire tower is built on a thick base plate (Fig. 14, 1" aluminum tooling plate) that features 4 precision drilled holes to position the first layer of spacer blocks and pins. The back sides of those 4 holes are counter-bored to house the swaged cable terminations. The plate also has a number of holes for attachment to the shaker.

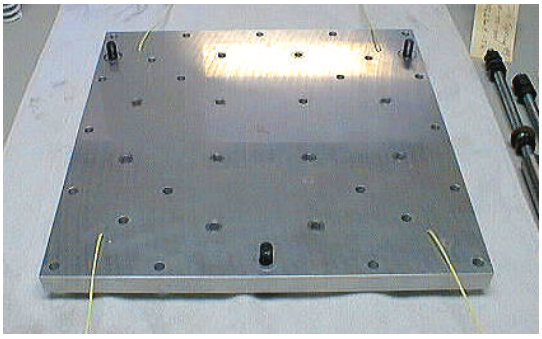

Figure 14: tower base plate ready for tower assembly, with kevlar cables in place.

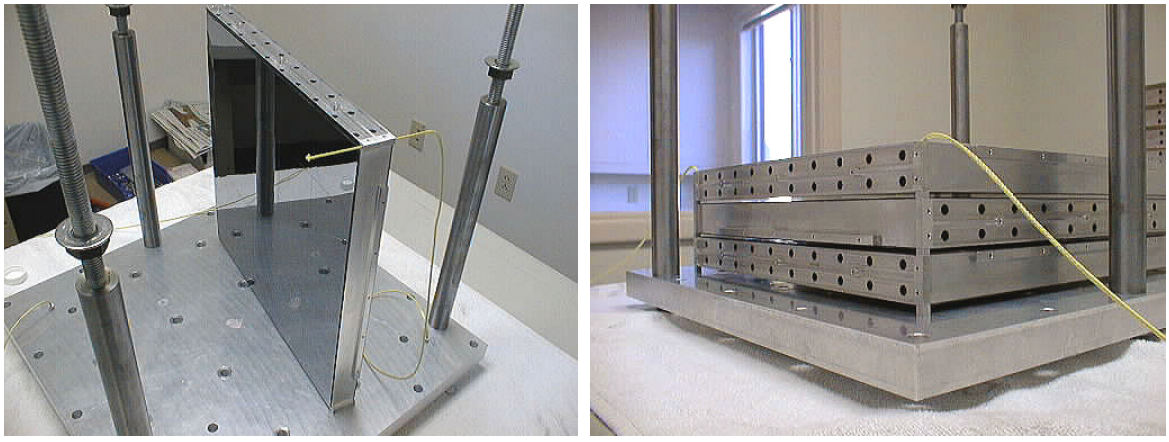

Figure 15: threading kevlar cable through a corner of the first tray left) and first 3 trays in place with kevlar cable running through corners.

Figure 16: tower assembly almost complete: kevlar cables held under prescribed tension by 4 compression springs.

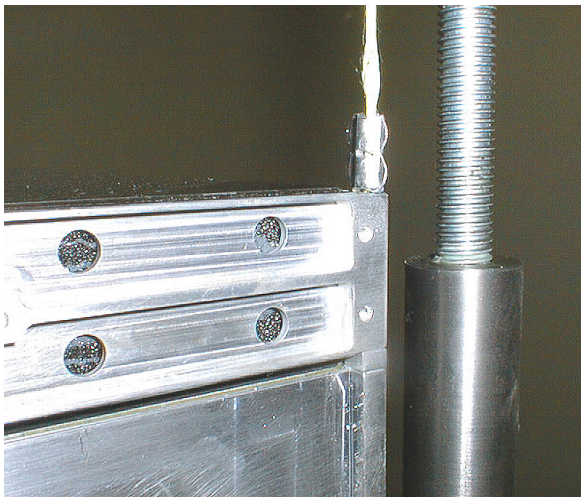

Figure 17: cable terminations are swaged in place while the cables are under tension; swelled section of cable above the swaged pieces is created by an insert in the cable intended to spread fibers apart, allowing better penetration of cyano-acrylate adhesive.

Trays are stacked one at a time, after threading the kevlar cables through the corner holes, spacer blocks, and pins (see Fig. 5). The end of the kevlar cables are stiffened with cyano-

acrylate glue to facilitate threading. This method of assembly proved extremely convenient and simple.

Once all 10 trays have been stacked, and swage blocks have been threaded on the cables at the top (but not yet swaged) a tensioning fixture is built on the base plate. The fixture consists of 3 posts with threaded rods at their top ends, supporting a thick (1") aluminum pulling plate. That plate can be raised with the sets of nuts that support it (Fig 16). The kevlar cables extend beyond the top of the tower, run through the plate and terminate at the top end of heavy duty compression springs. By pushing the plate up with the nuts, the springs are compressed and the cables put under tension. The amount of tension in each cable is easily measured by the amount of compression in the spring (the springs are sized so that this compression is about 1" and very easy to measure). Because kevlar creeps measurably when initially loaded, the cables and springs are kept under tension for several hours before securing the terminations at the top of the tower.

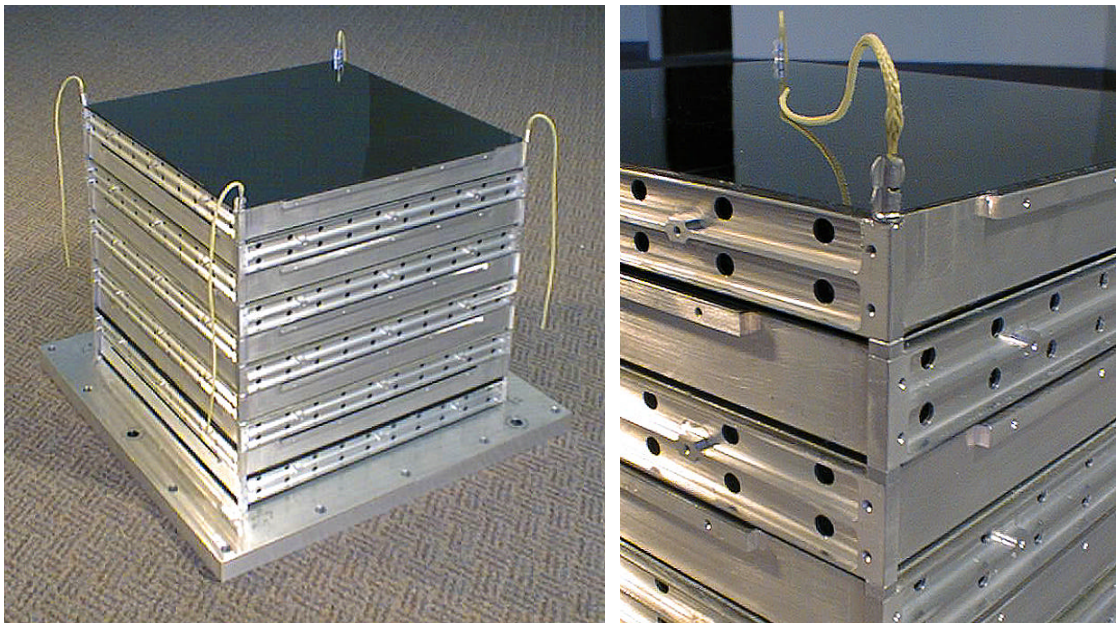

Figure 18: complete 10-tray prototype tower.

The finished tower is shown in Fig. 18. A quick survey of the stack revealed slight misalignments of some trays, consistent with the manufacturing tolerances imposed on the prototype hardware; the largest deviation from perfect alignment at the outer edges was about 100μm (.004") across the whole tower. More detail on tower alignment accuracy can be found in Section 7.4.

5. Experimental Setup and Test Plan

5.1 Shaker Equipment

All vibration tests were performed in house, on HYTEC's electro-dynamic vibration shaker system, shown in Fig. 19. The shaker (Ling Dynamic Systems 806LS) is mounted on an airbag-isolated "combo base" allowing horizontal shake tests on a 24×24 inch oil-film slip table,

in addition to the usual vertical tests. A 15×15 inch Magnesium alloy head expander is also available for use in the vertical direction. The shaker is air-cooled by a large suction fan and powered by an 8kVA solid state-amplifier (Ling Dynamic Systems DPA 8 DC).

The specifications for this system are:

- max. load: 3000 lbf 0-peak in sine operation or 2800 lbf RMS in random vibration
- max. travel: 2.0 inches peak-peak, in either vertical or horizontal directions.
- freq. range: DC to 2800 Hz
- max. velocity: 70 inches/second 0-peak in sine mode.

Both sinusoidal sweep and random vibration control are provided by a PC-based Data Physics[6] DP350Win Vibration Control System (3 inputs, 1 output). The random vibration controller shapes the base acceleration PSD to the required spectrum with a +/- 3dB tolerance (or +/- 41% on the RMS acceleration), and a 3-sigma clipping limit (i.e. peak acceleration at the base of the device being tested will not exceed 3 times the RMS value).

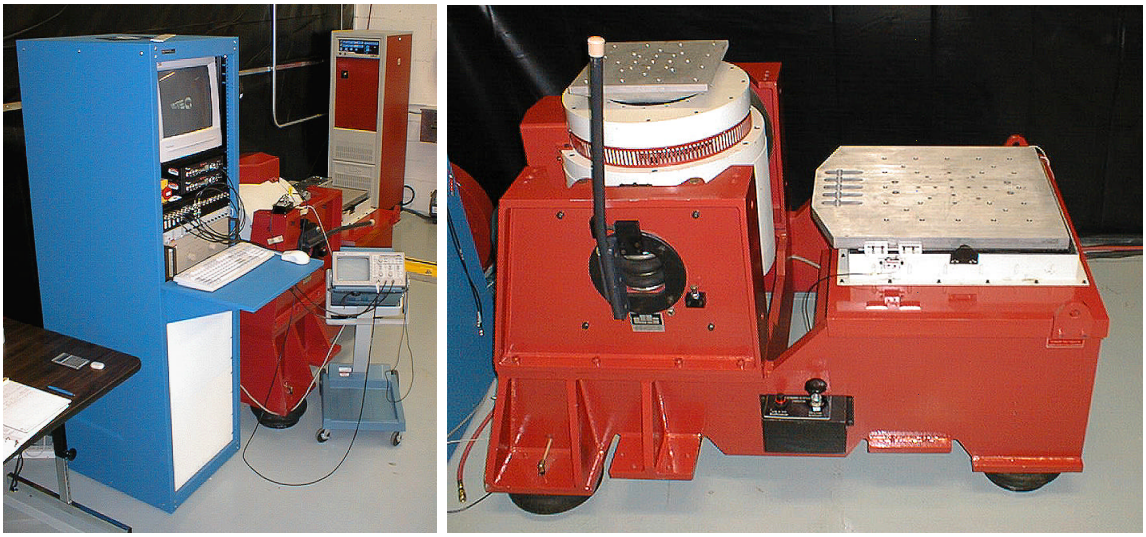

Figure 19: HYTEC s LDS 806LS/DPA8 horizontal/vertical electro-dynamic shaker system, and associated power amplifier, vibration controller, and data acquisition racks.

5.2 Measurement, Data Acquisition, and Post-Processing Equipment and Software

In all tests, the devices are instrumented with low impedance piezoelectric accelerometers (Kistler, various models), powered and conditioned by a 12 channel, line powered, conditioning module (Kistler 5124A1). The acceleration at the base of the device is always measured to serve as the feedback signal for the controller and as a reference for transfer function calculations. The other accelerometers are mounted at various locations on the device itself.

A PC-based data acquisition/FFT analyzer system was used to acquire the test data (DSP Technology[7] SigLab 20-42, 8 channels input, 4 channels output, 0-20 kHz). The analyzer is controlled directly from within Matlab[8] using a series of graphical VI's (Virtual Instruments). The data is then directly available for post-processing within Matlab.

For the tower tests, experimental mode shapes are reconstructed from sets of measured transfer functions using the commercially available Structural Dynamics Toolbox[9], working within the Matlab environment.

5.3 Test Plan

Two types of tests were performed: low amplitude modal tests intended to validate the modeling of the trays and tower, followed by high amplitude random vibration qualification tests to demonstrate survivability of the design to launch environments. Qualification tests were first performed with side-walls on; this provides a first confirmation of the design and modeling at a reduced risk of damage.

The tests are sequenced as follows:

1. Validation of single tray models: a single tray, without payload, is attached on the shaker (set for vertical tests) and driven with low amplitude white noise in the launch direction. The base (head expander) and the center of the tray are instrumented with accelerometers. This test will determine the first natural frequency ("drum mode") of the tray for comparison with predictions from the model; both the graphite/epoxy and the aluminum faced trays will be tested (one tray of each type).
2. Validation of tower model without side-walls: the tower is attached on the horizontal slip table of the shaker and driven with low-amplitude white noise; 8 accelerometers measure the motion of the base and 7 of the 10 trays. Post-processing provides natural frequencies, quality factors, and mode shapes of a few of the tower modes, for comparison with analytical predictions.
3. Measurements of tower dynamics with side-walls: same test as #3, but after attaching the side-walls on the tower. This test is intended to evaluate the impact of side-walls on the stiffness of the tower.
4. Transverse qualification test of tower with side-walls: with the tower attached on the horizontal slip table, and after defining an appropriate notching scheme (see Section 7.3), the random vibration qualification test spectrum is applied for 1 minute, first in the 0^o direction then in the 90^o direction (after rotating the tower 90^o on the slip table). A sub-miniature accelerometer measures the motion of the top tray. The frequency response of the structure is measure immediately before and after each test to try and detect structural changes and/or damages. The tower is also examined closely before, during, and after each test.
5. Transverse qualification tests of tower without side-walls: this test is similar to the previous one (#4) but with the walls removed.
6. Axial qualification test of tower without side-walls: the tower is attached on the shaker's head expander for a shake test in the launch direction. The random vibration spectrum is filtered to avoid over-exciting the numerous combinations of tray "drum" modes (see Section 7.3).

6. Tray and Tower Modeling and Response Predictions

This section describes modeling efforts intended to predict the response of the prototype trays and towers for comparison with test data. The models are representative of the "as-built" components, which, for some details are not necessarily identical to the "as-designed" structures. In particular, as was mentioned in the component descriptions, the corner pieces and spacer blocks were mistakenly chamfered instead of being left with sharp corners to maximize contact area. This reduced the contact area from 5.5x5.5mm to an estimated 3.5x3.5 mm. The models also use measured properties of the components (thicknesses, moduli, etc...) and include the mass of adhesives used in tray assemblies.

6.1 Mechanical Properties of Carbon Face Sheets

Mechanical properties of laminated composite plates are sensitive to the fiber volume fraction achieved by the manufacturer. Fiber properties themselves also have significant scatter. The plates were ordered as $0/-60/60|_S$, with XN50 high modulus graphite fibers in epoxy matrix, and a minimum required fiber volume fraction of 60%. The plates were expected to exhibit a quasi-isotropic Young's modulus of about 103 GPa (15 million psi).

	Expected	Measured
thickness	~ 300 μm	318 μm
mass/unit area	~ 0.5 kg/m^2	0.4793 kg/m^2
Young's Modulus, dir. 1	103 GPa (15×10^6 psi)	68.7 GPa (9.97×10^6 psi)
Young's Modulus, dir. 2	103 GPa (15×10^6 psi)	83.4 GPa (12.1×10^6 psi)

Table 4: mechanical properties of graphite/epoxy face sheets, expected and measured values; directions 1 and 2 are two orthogonal directions in the plane of the sheets.

Samples of the finished plates were cut in two orthogonal directions (1 and 2) and sent to a testing laboratory[10] for Young's modulus measurements. The tests were performed per ASME 3039 specifications. Table 4 summarizes the expected and measured stiffness and mass properties. The differences are most likely due to a low fiber volume fraction from manufacturing[11].

6.2 Mechanical Properties of RVC Foam Core

There is unfortunately very little data available on this material. A number of theoretical studies on mechanical properties of open cell foams give some guidance by correlating the foam's Young's and shear moduli (E, or G normalized to the moduli of the bulk material E_s, *or* G_s) to its relative density (the ratio of the foam density ρ to the bulk material's density ρ_s, also equal to the volumetric solid fraction in the foam). A simple model leads to

$$\frac{E}{E_s} = C\left(\frac{\rho}{\rho_s}\right)^2, \qquad (13)$$

where C is constant, usually assumed equal to unity[12]. A similar relation holds for the shear modulus. This also suggests that these elastic properties are essentially independent of pore size. Comparisons with experimental data shows reasonable agreement[12]; however the uncertainty on actual foam properties is still as wide as a full order of magnitude.

In the case of reticulated carbon foam (RVC), an added difficulty is that the properties of the bulk carbon itself are not well known (elastic properties of various forms of carbon vary widely).

Using those correlations however, we can get an idea of realistic ranges of Young's and shear moduli for a 3% volume fraction carbon foam (the 3% volume fraction is specified by the manufacturer and was verified experimentally at Hytec). The approximate ranges obtained with equation (13) are as follows:

$$\begin{aligned} &20\ \text{MPa} < E < 29\ \text{MPa}, \\ &7.5\ \text{MPa} < G < 11.2\ \text{MPa}. \end{aligned} \qquad (14)$$

The manufacturer of this foam also provides rough values for these properties, although admittedly not based on direct testing, and not itemized for various pore sizes. These specifications are[13]

$$31\,\text{MPa} < E < 62\,\text{MPa},$$
$$G \approx 30\,\text{MPa}, \qquad (15)$$

obviously not in very good agreement with the previous estimates.

Because static and dynamic response of our trays is particularly sensitive to the shear modulus of the foam, we decided to perform a direct measurement of this modulus. The experimental setup is essentially a single degree of freedom mass-spring system, where the mass is a well-known block of metal and the spring is a strip of foam, bonded to the metal block and to a rigid base, and deforming in essentially pure shear (for one dominant mode anyway). The setup is shown in Fig. 20. It is mounted on the horizontal shaker described in Section 5.1 and excited with white noise at very small amplitudes. Accelerometers measure the motion of the base and the top mass and an FFT analyzer is used to record the transfer function between those two signals.

An inverted piece of aluminum U-channel was used as the mass block to lower the center of mass closer to the shear center of the foam block; this minimizes the amount of pitch-shear coupling.

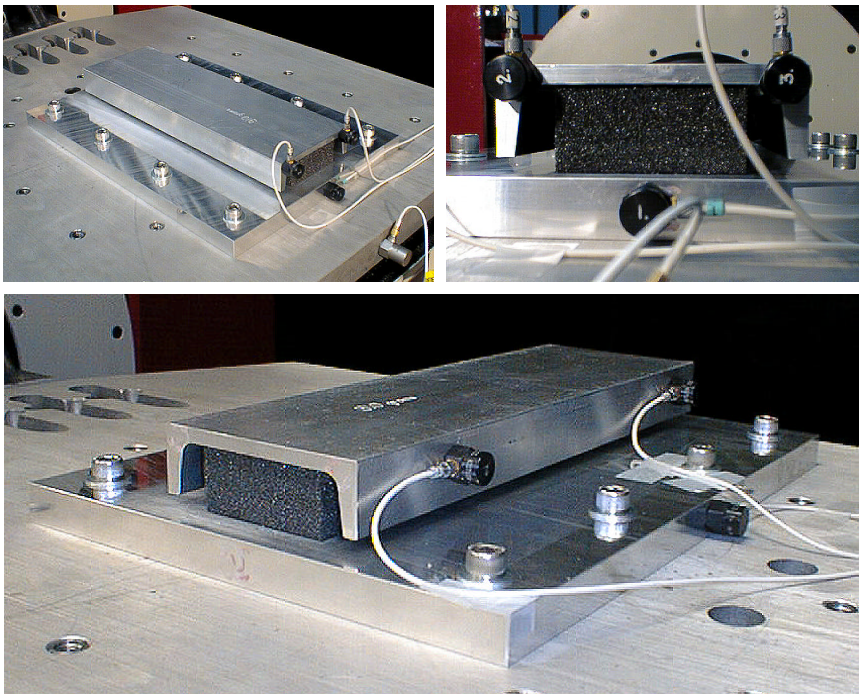

Figure 20: experimental setup for measurement of shear modulus of the RVC foam; test device is mounted on the shaker s horizontal slip table; clockwise from top left: setup for longitudinal shear mode measurement, detail of test sample, and setup for measuring transverse modes.

The foam block used in the test was cut to w = 2.50” wide by h = 1.15” thick by l = 12.55” long. The natural frequency of the longitudinal shear mode of the system is a direct measure of the shear modulus of the foam; it is given by

$$f_{shear} = \frac{1}{2\pi}\sqrt{\frac{GA}{hM}}, \qquad (16)$$

where f_{shear} is the natural frequency of the shear mode in the lengthwise direction of the test article, G is the shear modulus of the foam, $A=wl$ is the cross sectional area of the foam block in the shear plane, and M is the total mass of the aluminum channel and accelerometers (measured at 920 grams).

Figure 21 shows measured transfer functions from base acceleration to accelerations of the aluminum top piece as a function of frequency. Two curves are shown and correspond to longitudinal and transverse tests. Four modes can clearly be seen from 370 Hz to 571 Hz, and a group of possibly 3 modes between 809 and 862 Hz. Additional measurements were performed to identify the pure longitudinal shear mode as the 3rd peak in these curves. Its frequency is 537 ± 0.5 Hz. Solving (16) for G, one finds

$$G = 15.11\,\text{MPa} = 2.19\,\text{ksi}. \qquad (17)$$

The experiment does not provide a direct measure of the Young's modulus. However, the tray dynamic behavior is not very sensitive to that value. Assuming a Poison's ratio of 0.3, the Young's modulus would be

$$E = 39.3\,\text{MPa} = 5.7\,\text{ksi}. \qquad (18)$$

The test also provides an estimate of the Q (quality factor) of this foam in shear: modes #3 and #4 show a Q of about 80 to 100 (loss factor around 1%).

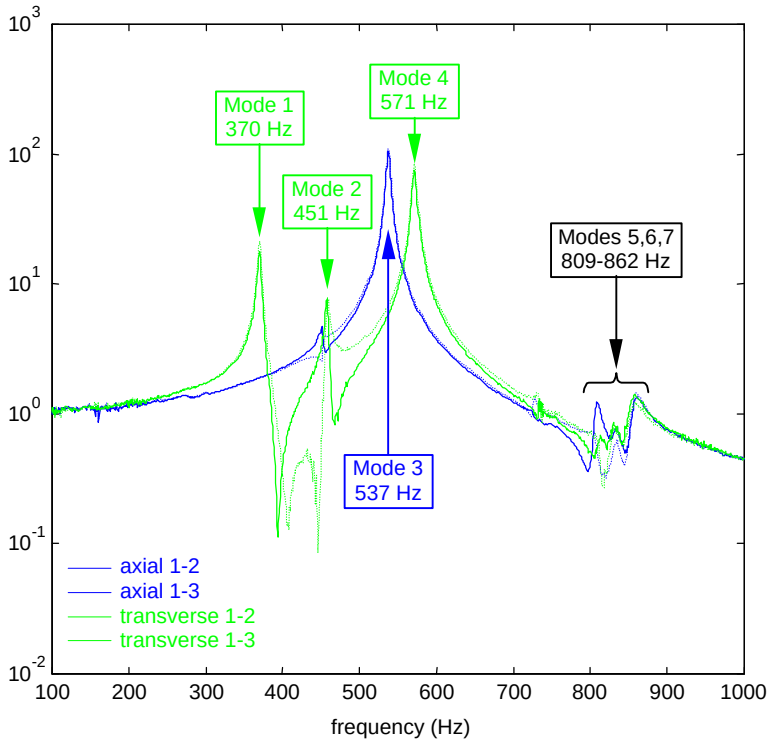

Figure 21: measured FRFs from base to mass block of foam test device; blue curves show axial FRFs, green show transverse FRFs.

To further confirm the validity of the moduli of Eq. 17 and 18, a finite element model of the test device was generated and the 7 lowest natural modes were calculated. The resulting natural frequencies are summarized in Table 5 and compared with measured values. The agreement is excellent, and confirms the validity of the assumption on the Poison's ratio. Fig. 22 shows the first 4 mode shapes obtained from the model.

Mode #	experimental freq. (Hz)	FEM freq. (Hz)	Model error (%)
1	370	396	+7.0
2	451	452	+0.2
3	537	527	-1.9
4	571	556	-2.6
5	~809	751	-7.2
6	~835	863	+3.4
7	~862	876	+1.6

Table 5: foam stiffness test: comparison of first six natural frequencies from FEM and experiment.

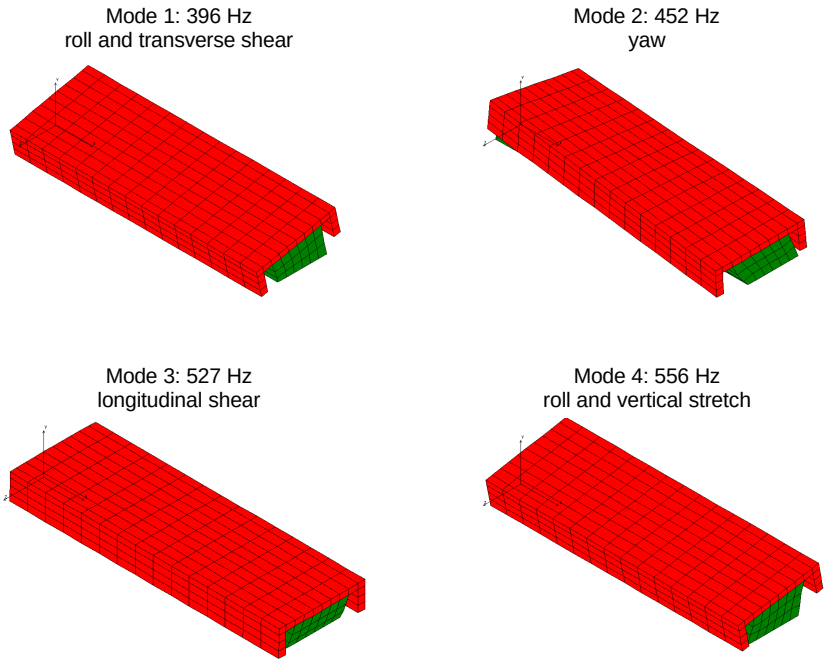

Figure 22: first 4 mode shapes from finite element model of the foam test device using *G*=15.1 MPa, and *E*=39.3 MPa; mode #3 is essentially pure longitudinal shear in the foam and provides a direct measure of the shear modulus.

6.3 Finite Element Models of Single Tray

A detailed finite element model of a single tray was generated. The model is shown in Fig. 23. The aluminum tray closeout frame is modeled with 8-node solid elements, except for the stiffening ribs which are modeled with 4-node shell elements. The foam core is represented with 8-node solid elements and the face sheets with 4-node shell elements.

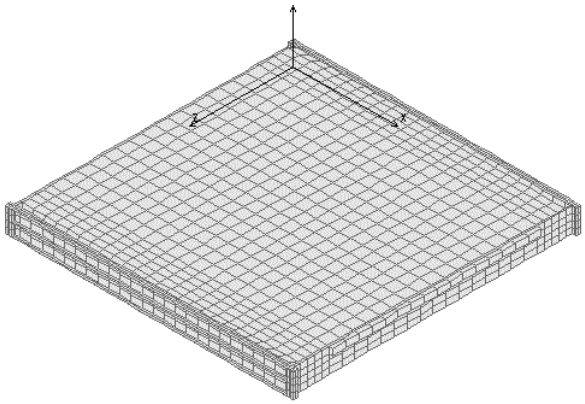

Figure 23: finite element model of a tray.

All elements in the model use isotropic properties; by selecting different property sets, the same model can be used to represent a tray with either aluminum or graphite/epoxy face sheets.

The mass loading corresponding to the payload is represented by increasing the density of the top and bottom face sheets in the model. Stiffness contributions from the payload are neglected (payload is made of discrete tiles, not continuous layers).

Mass distributions in the models were carefully checked and compared to measured values, including measured masses of adhesives used in the tray assemblies. Table 6 summarizes the mass breakdown for a typical tray (average values).

item	mass (g)
Structural	
aluminum closeout frame	240
RVC foam core block	159
face sheets (2)	100 (type B) / 162 (type B)
total epoxy for structural assembly	16
Total Structure	**515 (type A) / 577 (type B)**
Actual Payload	
lead converter tiles (25)	200
kapton sheet (2)	38
silicon chips (50)	250
total epoxy for payload	74
Total Actual Payload	**562**
Dummy Payload	
top aluminum tiles	100
bottom aluminum tiles	275
total epoxy for dummy payload	30
Total Dummy Payload	**405**
Totals - Finished Trays	
graphite/epoxy faces and actual payload (type A)	**1077**
aluminum faces and dummy payload (type B)	**982**

Table 6: mass properties break-down of typical prototype trays.

The model was used to predict the lowest "drum" mode of the tray, first without any payload (Tables 7 and 8). The boundary conditions are simple supports of the bottom side of

each corner. The predicted values are compared to measurements in Section 7.1 for validation of the models.

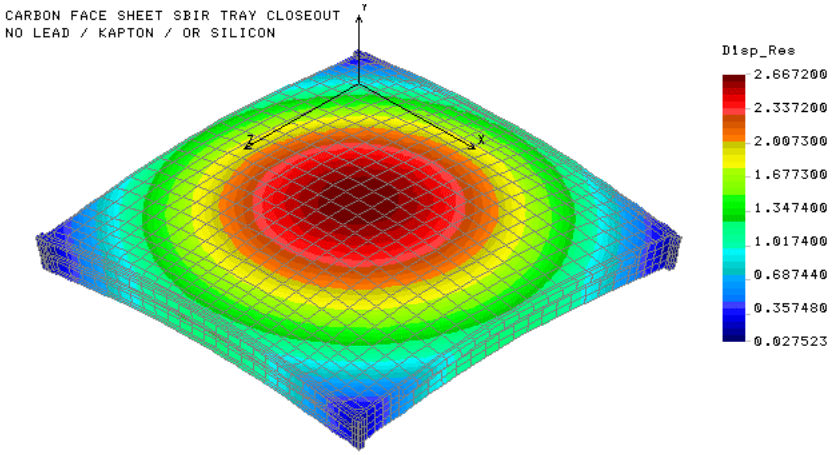

Figure 24: first natural mode of single tray supported at bottom of each corner; color code shows total displacement.

Core Properties	Face Sheet Properties	Frequency (Hz)
Vendor specs (*G*=4.4 ksi)	Vendor Specs (*E*=15 Msi)	642
Measured (*G*=2.2 ksi)	Vendor Specs (*E*=15 Msi)	599
Measured (*G*=2.2 ksi)	Measured (*E*=11 Msi)	557

Table 7: predicted first natural frequency of simply supported tray with graphite/epoxy face sheets (Type A, no payload); comparison of results with vendor listed and measured material properties.

Core Properties	Face Sheet Properties	Frequency (Hz)
Vendor specs (*G*=4.4 ksi)	6061-T6 (*E*=10 Msi)	540
Measured (*G*=2.2 ksi)	6061-T6 (*E*=10 Msi)	499

Table 8: predicted first natural frequency of simply supported tray with aluminum face sheets (Type B, no payload); comparison of results with vendor listed and measured material properties.

The payload is then added to the model (neglecting any stiffness contribution) as a mass loading at the surfaces of the tray. The resulting natural frequencies are listed in Table 9.

Tray Type	Frequency (Hz)
A (GRFP face sheets & realistic payload)	335
B (aluminum face sheets and dummy payload)	350

Table 9: predicted first natural frequency of simply supported tray with payload.

6.4 Finite Element Model of Complete Tower

A finite element model of the complete 10-tray tower was created in Cosmos (Fig. 25). The individual trays are modeled as explained above, and 10 of these models are stacked to represent a tower. The corner spacer blocs are modeled with a reduced contact area by removing a number of elements at their periphery (see Fig. 27).

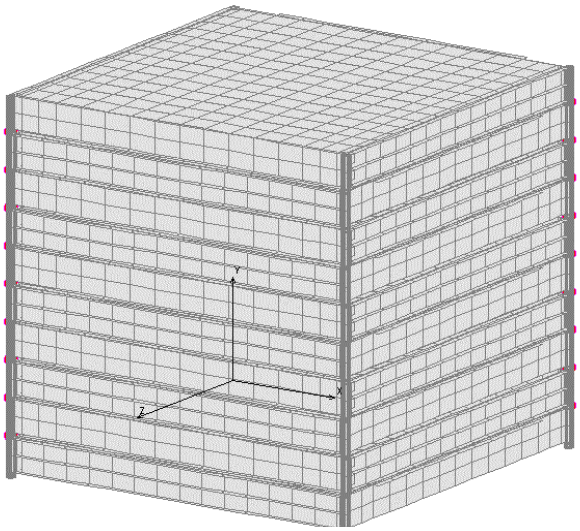

Figure 25: FE model (COSMOS) of the complete prototype tower (without side-walls).

The model is used to predict static deflections and stresses as well as natural mode shapes and frequencies. Results for deflections and stresses are presented in the next section. Predicted mode shapes and natural frequencies are shown in Fig. 26. Those predictions are compared with measurements in the Test Section.

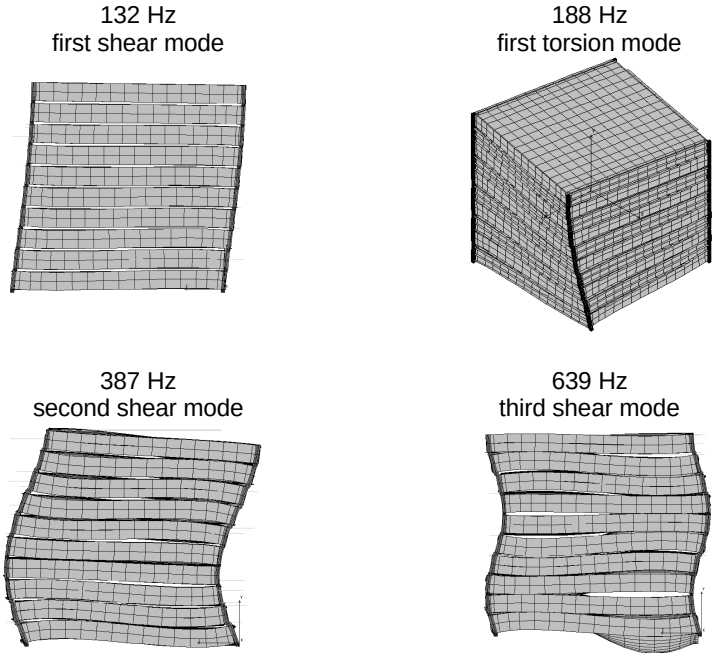

Figure 26: four global modes of 10-tray tower without walls, as predicted with COSMOS model.

Note that a large number of tray modes (various phase combinations of drum modes in all 10 trays) are predicted starting at 306 Hz. These modes are not shown in Fig. 26.

6.5 Static and Dynamic Deflections and Stresses

A hand calculation for static corner stresses was presented in Section 3.3. This calculation can be repeated, this time accounting for the reduced contact area between the corner blocks and the tray closeouts (i.e. c=3.5mm instead of 5.5mm). The calculated stress level is then 125 MPa (up from 47 MPa with full contact), and the safety factor is reduced to about 2 (down from 5.4 with full contact).

Static stresses can be obtained from the full tower Cosmos FE model of Fig. 25. The model is "loaded" with static acceleration levels of 10*g* downward and 4*g* transverse. The largest stresses occur at the interface between corner blocks and tray frames, in the lower stages of the tower. The results are shown in Fig. 27. The largest stress is about 38 MPa and is mostly compressive. Note that this value does not include the additional compressive stress from the tension in the cables which is approximately 934 N (210 lbf) over $(3.5\ \text{mm})^2$, or about 76 MPa. Adding those two contributions, the maximum total stress is about 114 MPa, in excellent agreement with the hand calculated value.

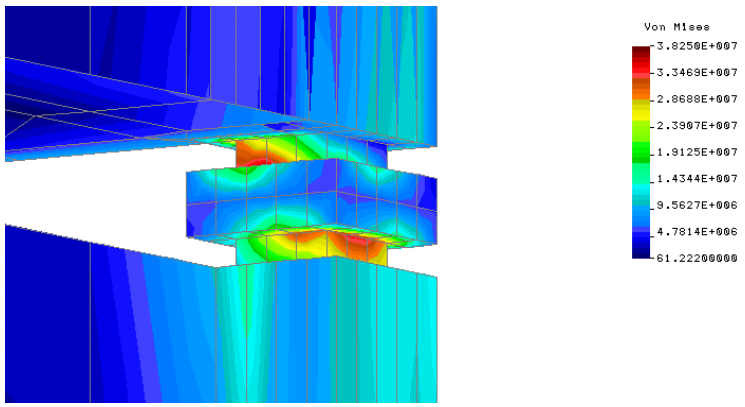

Figure 27: pseudo-static corner stresses from Cosmos FE model, for full tower under 10*g* down + 4*g* transverse; initial stress from cable tension not included.

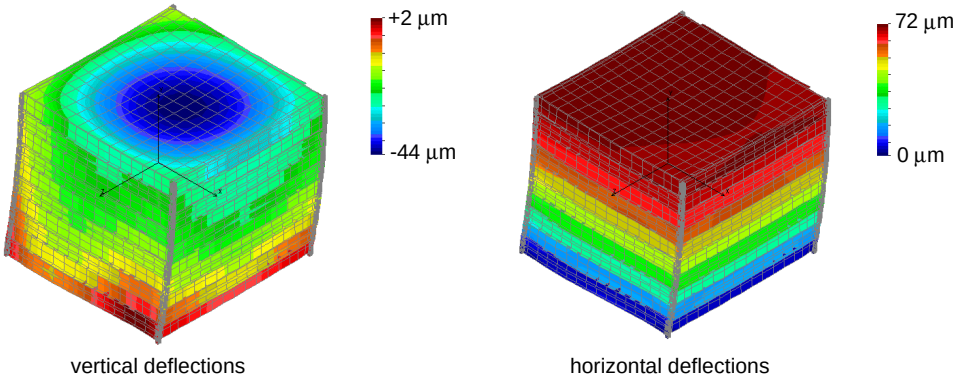

Figure 28: static deflections from Cosmos FE model, for full tower under 10*g* down + 4*g* transverse.

Static deflections for the same load case are shown in Fig. 28. The largest transverse deflections occur at the top of the tower and amount to about 72µm. The trays themselves deform out of plane in reaction to the 10*g* vertical loading. The maximum deflection occurs at

the center of the trays and amounts to about 44μm. The gap between silicon chips on consecutive trays is nominally 1.5 to 2mm; accounting 2×0.5mm for wire bonds, this leaves about 500 microns of open clearance, to be shared by 2 trays, or an upper limit on tray deflection of 250 microns.

Predicting dynamic stresses under random vibration inputs is significantly more difficult. As mentioned above, our goal for the second phase is to make use of the lumped parameter models to perform those calculations.

Without numerical simulations, it is possible to obtain an estimate of the order of magnitude of dynamic stresses in random vibration by comparing deflections under random vibrations to static deformations under transverse accelerations. The response of a multi-degree-of freedom system to "almost" white random vibration inputs is typically dominated by the response of the fundamental mode (at least as far as deflections are concerned; this does not necessarily hold true for stresses). Also, the fundamental mode shape is often very similar to that of the static deflection; this is true in this case where the first shear mode of the tower is very similar to its deflection under transverse acceleration.

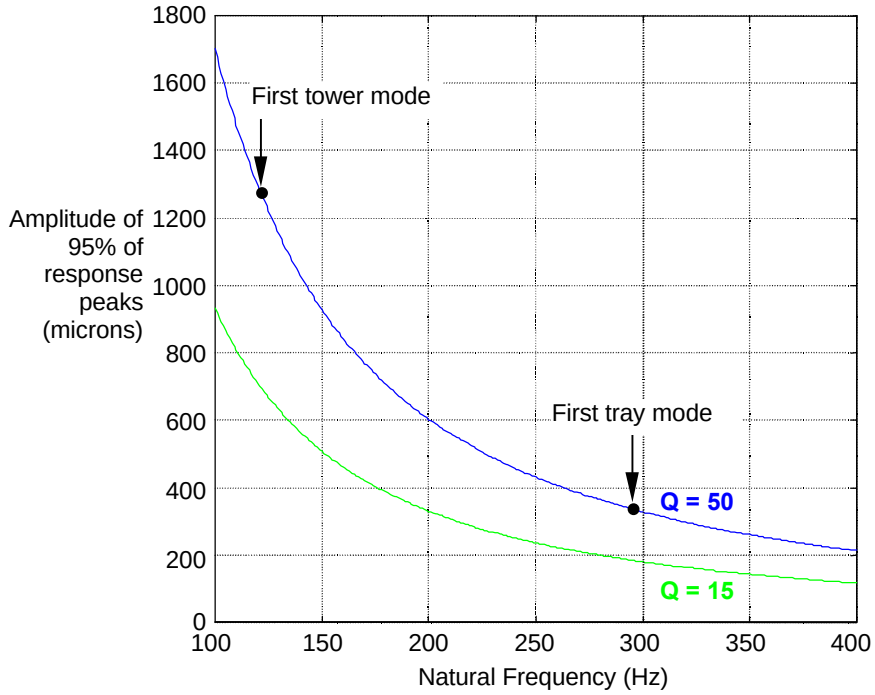

Figure 29: approximate dynamic deflection of the fundamental mode of a structure in response to random vibration at the base (0.15 g^2/Hz) as a function of the fundamental frequency and Q of that mode.

The amplitude of response (approximately equal to the motion of the top tray relative to the base, noted u) of the first mode of the tower to random vibration at the base follows a narrow band process and can be evaluated based on single degree of freedom models as[14]

$$\sigma_u = 0.3114\sqrt{\frac{QW_a}{f_n^3}}, \qquad (19)$$

where σ_u is the standard deviation of the deflection (or its RMS value), in meters, Q is the quality factor of the mode, W_a is the power spectral density of the base acceleration (g^2/Hz), and f_n is the

natural frequency of the mode in Hertz. An upper bound on the deflection can be calculated with any given confidence level using the error function[14]. The results are shown in Fig. 29, where a deflection not exceeded by 95% of the cycles ($\approx 2\times\sigma_u$) is plotted as a function of the fundamental frequency and Q of the structure considered.

Looking at Fig. 29, it is clear that a lightly damped tower (a *Q* of 50 is typical for this type of structures) with a fundamental frequency around 120 Hz can respond with very large deflections (about 1.3 mm) to the random vibration qualification test planned. Note also that a 1.3 mm deflection is about 18 times more than the static deflection under 4 *g*, for which the tower was designed (with a safety factor of 2 on stresses with 3.5mm contact areas). To avoid failure (and because the random vibration qualification test is intended for workmanship verification and not as a simulated launch) a standard practice consists of "notching" the random vibration spectrum to reduce the energy in narrow frequency bands around known resonances. Details of the notching technique and its application in the tower tests can be found in Section 7.3.

The figure also shows the expected dynamic deflection of the trays, under random vibration in the launch direction: about 350 microns, which also exceeds the limit (250 microns) to avoid damage.

6.6 Lumped Parameter Dynamic Models

HYTEC has developed a proprietary software for lumped parameter modeling of 3-dimensional dynamic systems. The software is written in the MATLAB language. By design, it allows rapid exploration of parametric variations of the system and their effect on dynamic behavior.

The lumped parameter modeling technique represents the system as a 3-dimensional network of mass elements (with rotational inertia) and 3-dimensional springs with any combination of viscous and structural damping. The spring properties (stiffnesses and damping) can be entered as frequency dependant values (essential to accurately model visco-elastic damping).

Models of single trays and complete towers have been generated and were used as tools to lead the design of those structures. Once complete FEM models were also available, the modeling assumptions were further refined and a couple of empirical modeling parameters were adjusted (one for the tray model and one for the tower model).

Even though this Phase I design was based on static design load factors, the models were validated so they can be used in Phase II to explicitly evaluate random vibration response (stresses, deflections,...), which would be impractical with the finite element models because of CPU time consumption (a full tower solution in COSMOS requires several hours CPU on a Pentium PC, while the MATLAB model of a complete tower runs in a few seconds).

The models and some simulation results are presented in the corresponding test sections.

7. Vibration Test Results

7.1 Single Tray Modes

As a first attempt to validate our models, we measured the fundamental frequency of a single trays (one with graphite epoxy face sheets or type A, and one with aluminum face sheets or type B), and without payload (lead, kapton, or silicon). The tray is attached to a base plate with 4

short pieces of kevlar cable, tensioned to about 200 lbf. Four corner spacer blocks are used to support the corners. Those blocks are sitting on stiff standoffs to provide access to both sides of the tray.

This assembly is attached on the shaker (Fig. 30) and excited with low amplitude white noise acceleration. The base plate and the center of the tray are instrumented with accelerometers. Transfer functions from the base to the tray center-point are measured with the FFT analyzer to identify the frequency of the "drum" mode.

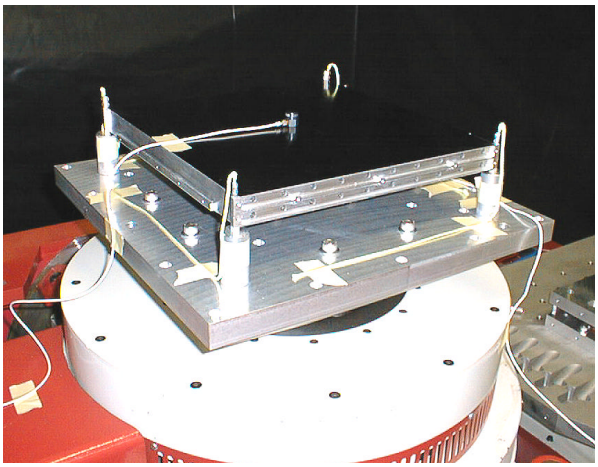

Figure 30: single tray undergoing tests for first resonant mode (drum mode).

The results are shown in Figs. 31 and 32, for the type A and B trays, respectively. The measured natural frequencies and Q's are also listed in Table 10 and compared to results from the Cosmos models. The agreement is satisfactory. Note that we later determined that the mass of the accelerometer (which was not include in the models) reduces the natural frequency by about 25 Hz. The rest of the difference is believed to be due to flexibility of the large head expander that had to be used on the shaker.

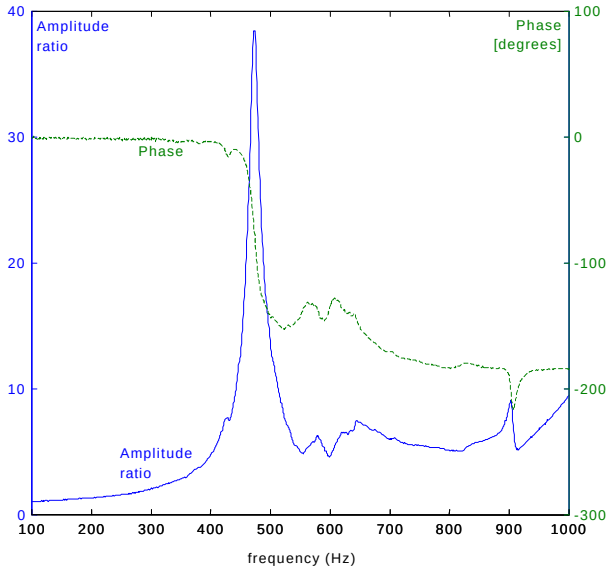

Figure 31: measured transfer function from base to center for a type A tray (graphite/epoxy face sheets) without payload.

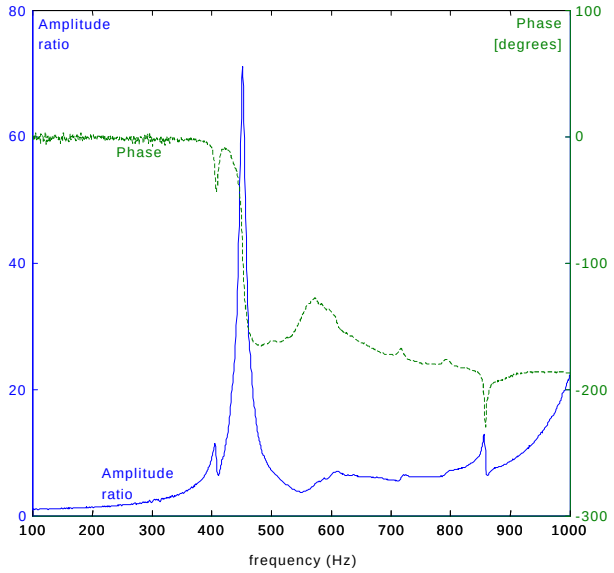

Figure 32: measured transfer function from base to center for a type B tray (aluminum face sheets) without payload.

Tray type	Cosmos FEA (Hz)	Experimental (Hz)
A (graphite/epoxy face sheets)	557	473
B (aluminum face sheets)	499	451

Table 10: predicted first natural frequency of simply supported tray with aluminum face sheets (no payload); comparison of results with vendor listed and measured material properties.

A 6 degree of freedom lumped parameter model was adjusted based on these results. The first 3 modes predicted by this model are shown in Fig. 33. This simple model was used as a building block for a Matlab model of a complete tower.

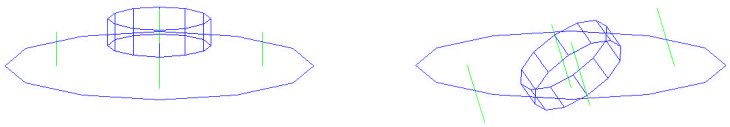

first mode ('drum'): 473 Hz

second and third modes: 669 Hz

Figure 33: mode shapes from Matlab model of a single type A tray without payload.

7.2 Tower Modes

This section describes a series of tests performed on the complete tower to identify natural modes and validate analytical models. The tower is tested first without and then with side-walls and in each case, the test data is post-processed to extract natural frequencies, quality factors, and mode shapes. Those experimental results are also compared to analytical predictions. In addition, lumped parameter dynamic models (in Matlab) are adjusted to represent the dynamics of the system.

7.2.1 without side-walls

The tower is first tested without side-walls (Fig. 34). It is mounted on the horizontal slip table of the shaker and instrumented with a total of 8 accelerometers: 1 at the base, and the rest on the 7 higher trays in the tower (#4 to #10). All accelerometers are measuring motion in the shake direction (i.e. horizontal). The base is excited with very low amplitude white noise and transfer functions from base to trays are recorded with the FFT analyzer.

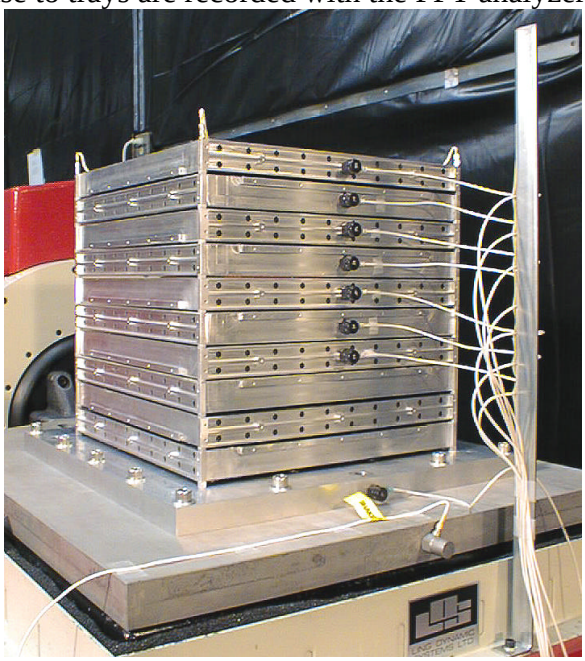

Figure 34: experimental setup for modal test on tower without side-walls.

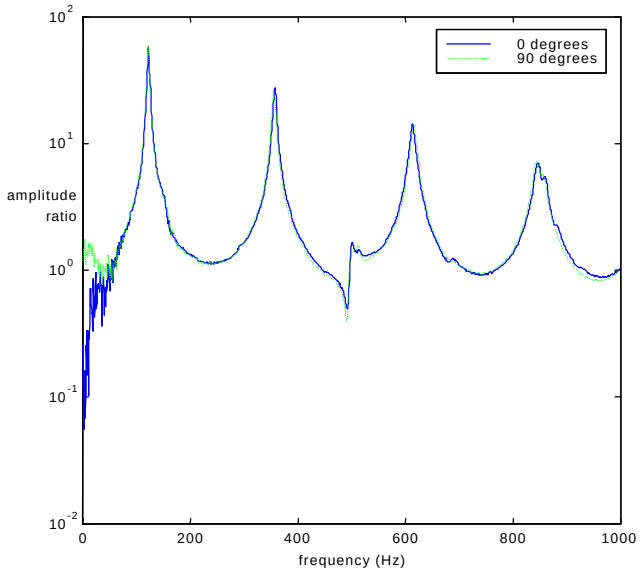

Figure 35: tower without walls; transfer function from horizontal base motion to horizontal motion of top tray (#10); comparison of response in 2 principal directions.

Another goal of the test was to detect any asymmetries in the tower dynamics. For this, transfer functions were measured in 2 orthogonal directions (the tower was rotated 90 degrees on the slip table). Two of these transfer functions are compared in Fig. 35; they are virtually identical, as expected.

The transfer functions were post-processed to extract mode shapes, natural frequencies, and damping. Those values are listed in Table 11 and compared with finite element results from Matlab and COSMOS models. Agreement is excellent. Note again that the COSMOS model *assumes* a 3.5x3.5 mm contact area between spacer blocks and tray frames and that the tower modes are very sensitive to this assumption.

	Experimental		Matlab	Cosmos
mode	***f* (Hz)**	***Q***	***f* (Hz)**	***f* (Hz)**
first shear	122	34	124	132
first torsion	-	-	195	188
various tray "drum" modes	293 & up	~40	255 & up	306 & up
second shear	358	60	366	387
second torsion	-	-	580	560
third shear	614	58	606	639
fourth shear	848	41	829	-

Table 11: tower without walls; experimentally identified modes (frequencies and quality factors) compared to FEM simulation results; note that some modes could not be measured experimentally with the accelerometer locations and directions chosen.

A lumped parameter model of the tower (Fig. 36) was also created by assembling 10 of the single tray models of Fig. 33 and semi-empirical elastic representations of the corner blocks. The stiffness values used in those models for the corner blocks are calculated from simplistic beam theory, with *one* adjustable parameter: the "effective" length of the beam corresponding to a corner block. This parameter can be adjusted such that the model predicts a fundamental frequency for the tower that is close to the FEM value or – if available – a measured value. The natural frequencies predicted by the adjusted model are listed in Table 11; the model itself and three lateral mode shapes are shown in Fig. 36.

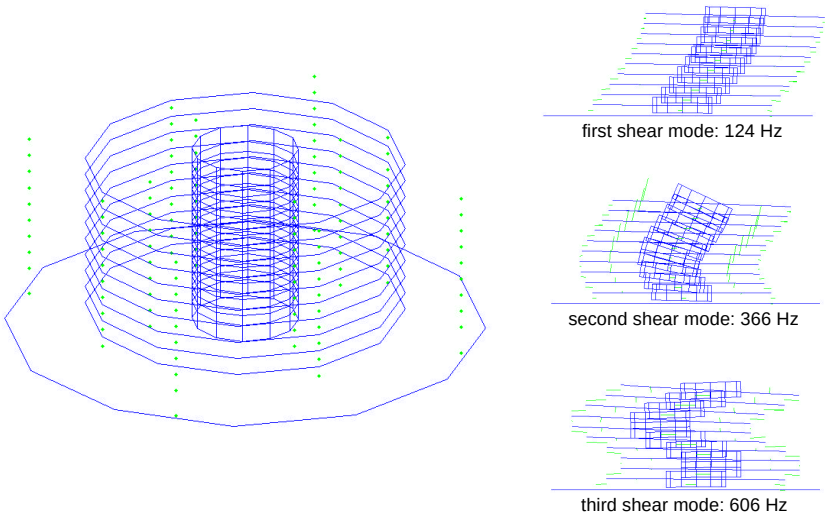

Figure 36: Matlab model of a 10-tray tower (left) and three transverse modes predicted by that model (right).

Once this adjustment has been performed for a particular design, the model can be used to analyze the effects of various but small design changes (or adding more layers for example). Because the Matlab models are entirely parametric and use only a few degrees of freedom (120 for a full tower) such trend studies can be performed very efficiently (each run takes only a few seconds on a Pentium PC). Such studies cannot practically be performed based on FEM models because of the prohibitive CPU time involved (several hours for a modal analysis on a Pentium PC). One must keep in mind however that drastic design changes can change the deformations enough that the adjusted value of the empirical parameter is no longer valid.

The adjusted model may also be used to calculate random vibration response and in particular stress levels, residual contact pressure at interfaces in the stack, and dynamic deflections of components. This was not done in Phase I but will become an important tool in Phase II. As an illustration of the type of random response calculations that can be performed with these models, Fig. 37 compares the 7 measured transfer functions to the corresponding simulation results. With the exception of a small systematic error on frequencies and inaccuracies in a number of anti-resonances (anti-resonances are notoriously difficult to predict since they are very sensitive to small changes in mode shapes, damping , and frequencies), the agreement is good.

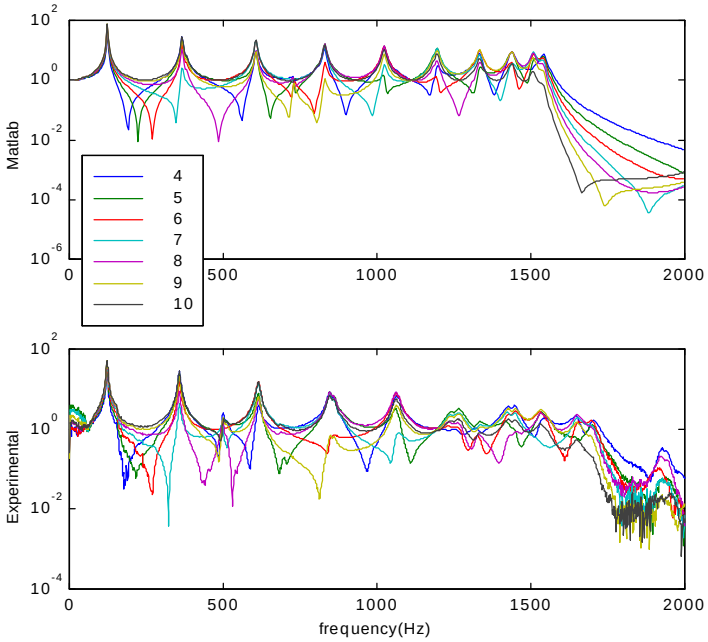

Figure 37: tower without walls; comparison of calculated (Matlab model) and measured horizontal FRFs from base to various trays.

The mode shapes identified from experimental data are compared to predictions from both the Cosmos and the Matlab models in Fig. 38; the agreement is clearly excellent.

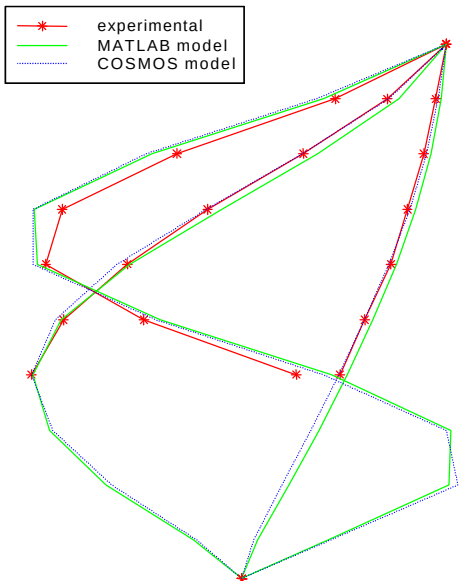

Figure 38: tower without walls; experimental mode shapes calculated from measured transfer functions compared to mode shapes from Matlab and Cosmos models.

7.2.2 with side-walls

The same tests were performed again after mounting the side-walls on the tower. The setup is shown in Fig. 39.

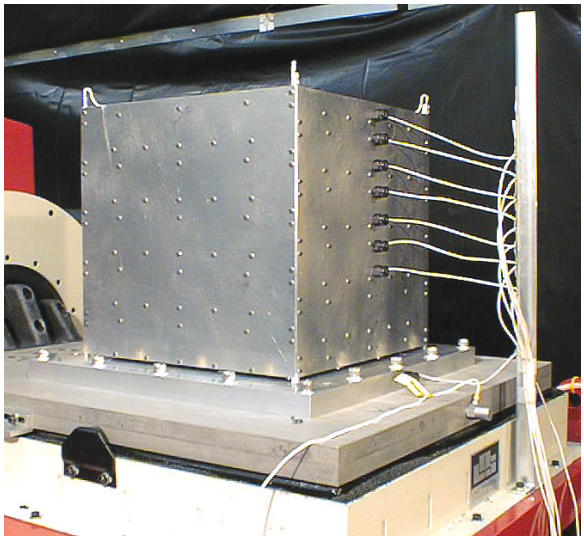

Figure 39: experimental setup for modal test on tower with side-walls.

In this case, because the corners of each tray are attached to only 2 walls, and this pattern repeats itself along the tower in alternating direction, one expects a difference in frequency

response in the two principal directions. The difference is due to a more direct coupling from the side-walls to the base in one direction than the other. This is confirmed in Fig. 40 that compares base-to-top transfer functions measured in the 2 directions.

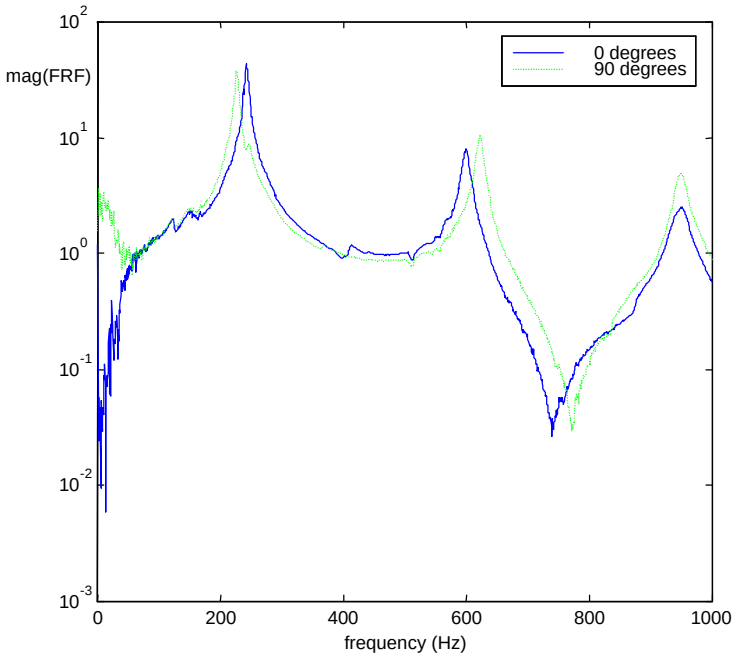

Figure 40: tower with walls; transfer function from horizontal base motion to horizontal motion of top tray (#10); comparison of response in 2 principal directions.

Natural frequencies and quality factors extracted from experimental data are listed in Table 12 and compared to predictions from the Matlab Models (in Phase I, Cosmos FE simulations were not performed for the tower with walls). Note that the walls are modeled very approximately in the Matlab models. The walls were added to the existing model of Fig. 36, without re-adjusting any empirical parameter. Note that the Matlab simulations still give a good estimate of the effect of the walls, even if natural frequency predictions for the higher modes are significantly off.

	Experimental		MATLAB
mode	***f* (Hz)**	***Q***	***f* (Hz)**
first shear/bending	243	38	271
first torsion	-	-	421
second shear/bending	600	55	1100
third shear/bending	952	37	not found

Table 12: tower with walls; experimentally identified modes (frequencies and quality factors) compared to simulation results from Matlab model (lumped mass) model; note that some modes could not be measured experimentally with the accelerometer locations and directions chosen.

Experimental mode shapes are shown in Fig. 41 and compared to Matlab predictions; the agreement is clearly excellent. Clearly, most of the deformation is now in the layer of spacer blocks between the base plate and the lower tray (#1). Note that, in an actual tower design with

side-walls, the lowest tray would be anchored directly into the supporting structure, with full contact all around the tray sides, and without the use of spacer blocks. Spacer blocks were used at the bottom stage of this prototype for lack of time in designing and building a different lower tray for direct anchoring.

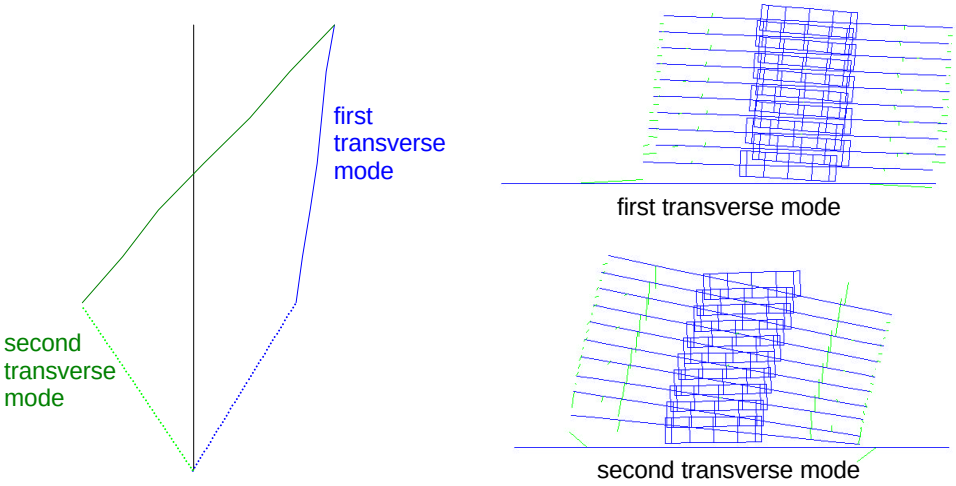

Figure 41: tower with walls; first two experimental mode shapes (left) calculated from measured transfer functions; note that lowest straight line segment is due to lack of accelerometer pickup on trays 1 to 3; 2 mode shapes predicted by Matlab models shown at right.

The results show that the addition of structural side-walls increases the tower stiffness by a factor 4 in the test configuration (i.e. with a "soft" support of the bottom tray on corner blocks). The same models predict a factor 30 increase in stiffness for a tower with a fully anchored bottom tray, as compared to a tower without walls (first transverse mode at 683 Hz).

7.3 Random Vibration Qualification Tests

The tower was subjected to a typical random vibration qualification test for space launched equipment. The particular test profile was taken from NASA's *General Environmental Verification Specification (*GEVS*)*[15], table B-2, page B-3 of appendix B. The specification is a blanket random vibration test level to be used for workmanship tests of components to be launched on the Space Transportation System (STS), in the absence of test and/or simulation data for the actual random vibration levels experienced by the particular component. Note that this test level is in general much harsher than what the component would experience in flight: random vibration levels at various locations in the spacecraft/instrument are attenuated by the dynamics of whatever structures connect that location to the source(s) of the vibrations.

The test profile is shown in Fig. 43. NASA requires testing the components at that level (+/- 3 dB) for 1 minute along each of 3 orthogonal directions[1].

Components subjected to such random vibration tests typically exhibit a number of discrete resonant frequencies within the test range (20 to 2000 Hz). Unless those resonances are highly damped, the response amplitudes at those discrete frequencies can reach extremely high

[1] Note that the GEVS shows the RMS *g* level for this profile to be 12.9*g* RMS; our calculations, using the specified PSD show a total of 13.8*g* RMS; we assumed the PSD breakpoints to contain the correct numbers, so that our tests were based on 13.8*g* RMS.

levels (see Section 6.5). Such levels are almost always in excess of failure limits. To avoid over-exciting the resonant modes of the test devices, a standard practice consists in *notching* the base acceleration PSD to eliminate most of the energy in narrow frequency bands around known resonances. This practice does not significantly affect the total RMS acceleration imposed on the item and is consistent with the intent of the test, i.e. discovering workmanship defects (the test is NOT a simulation of the actual launch environment).

In transverse tests of the prototype tower, notching was used to avoid overexciting the few (3 with walls and 4 without), high Q (about 40), dominant transverse shear/bending modes. The frequencies of those modes are measured immediately before the workmanship test is performed, and the results are used to define an appropriate notching scheme (see specifics below).

Testing the tower in the launch direction presents a different problem: the tower dynamics in the launch direction contains a very dense array of tray bending modes (various phase and amplitude combinations of drum modes in all trays) starting at about 300 Hz. Notching for these modes is not a viable option for two reasons. First, we did not instrument the tower for an accurate characterization of those modes (external accelerometers are not an option because the trays are too close to each other), and second, those modes are so numerous and closely spaced that notching would remove most of the energy above 300 Hz.

As an alternative, we followed another common approach to defining component test levels: using simulations of the spacecraft dynamics to determine more realistic vibration levels at the component's location. Note that, even though the "spacecraft" is completely hypothetical in this case, spacecraft design requirements impose lower limits on their natural frequencies, when anchored to the launch vehicle. Because spacecraft design is always mass driven, spacecraft/instrument combination designs tend to satisfy those requirements with little margin. The lowest natural frequency then essentially defines the attenuation of the vibration levels from spacecraft flexibility.

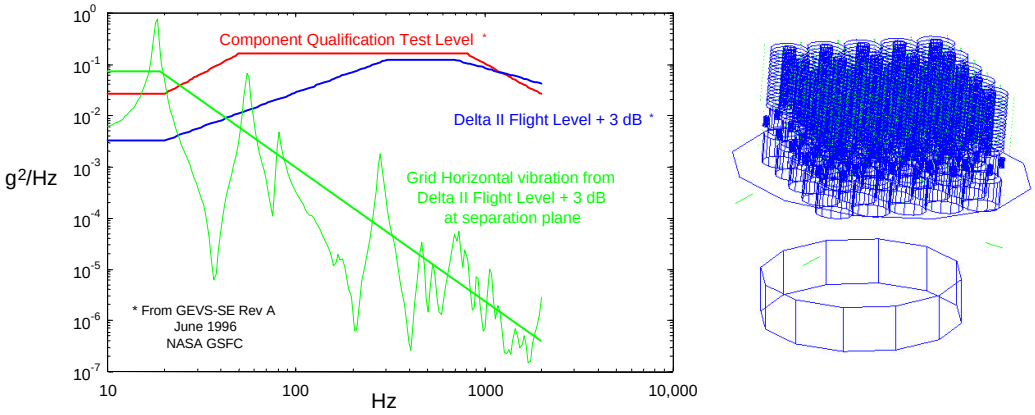

Figure 42: example of vibration attenuation through the spacecraft structure: random vibration level reaching the base of the GLAST trackers calculated with lumped parameter dynamic model shown at right of figure.

In addition, in this particular instance, HYTEC had already performed rough dynamic modeling of spacecraft/instrument configurations as part of the GLAST project. Those models can also be used to get an idea of attenuation. The GLAST trackers are very similar in concept to our prototypes; in GLAST, they are mounted on a stiff grid-like structure that also houses heavy

Cesium-Iodine calorimeters. With that configuration, most of the instrument mass is concentrated at the base of the trackers, so that base vibration levels exciting the trackers are strongly attenuated and only weakly dependent on the exact dynamics of other components.

Some results from these simulations are shown in Fig. 42. The dashed green curve is a dynamic simulation result for the random vibration PSD at the grid (the base of the trackers), resulting from random vibration input at the separation plane. The calculation assumes a Delta II launch vehicle and a nominal spacecraft, satisfying Delta II requirements of 12 Hz lateral and 35 Hz axial resonances. The figure also shows the lumped parameter dynamic model used. The figure shows that the "filtering" through the spacecraft is approximately –30dB/decade ($1/f^{1.5}$) above the lowest natural frequency of the system. Note that a single degree of freedom mechanical filter would give a 40dB/decade rolloff (or $1/f^2$). The difference is due to a number of additional resonances. We decided to assume an attenuation of –20 dB/decade ($1/f$) to define the test levels. This gives much larger vibration accelerations than expected in an actual system. The cutoff (i.e. natural frequency in the launch direction) was assumed to be 35 Hz (typical of the requirements imposed by launch vehicles). The resulting spectrum is detailed in Section 7.3.3.1.

7.3.1 transverse test with side-walls

7.3.1.1 Notched Vibration Spectrum

The base acceleration PSD as defined in the GEVS is notched to avoid over-exciting the first 3 natural modes of the tower with side-walls. The depth of the notches was set equal to $1/Q^2$, with Q=40, such that the resonant peaks in the tower response are essentially eliminated. The resulting spectrum is shown in Fig. 43.

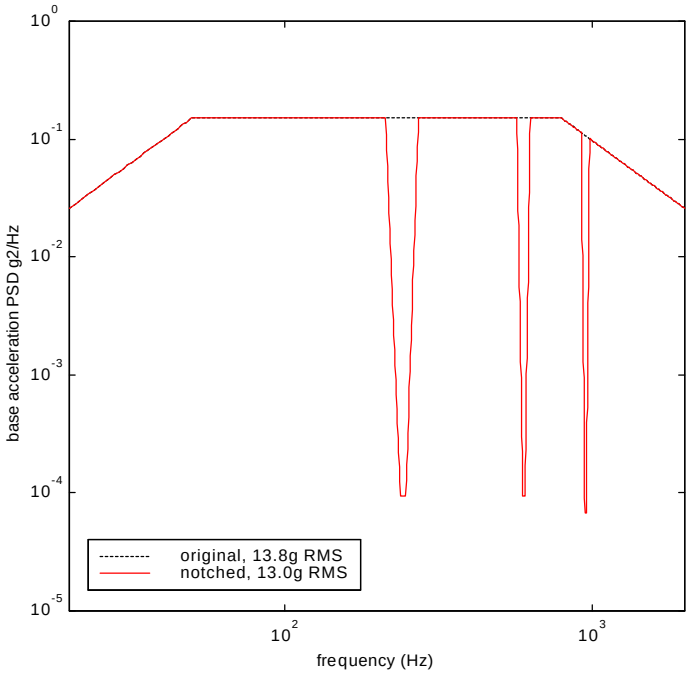

Figure 43: tower with walls; random vibration acceleration PSD notched to avoid excessive excitation of tower bending modes.

Figure 44 shows the measured base acceleration PSD during the test; it is maintained within +/-3dB of the required spectrum by the vibration controller.

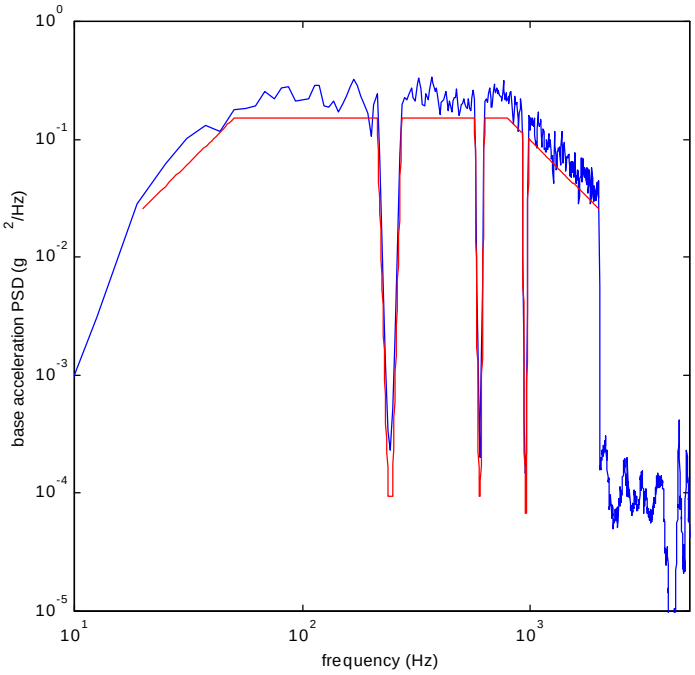

Figure 44: tower with walls; random vibration acceleration PSD notched to avoid excessive excitation of tower bending modes; measured PSD compared to required PSD.

7.3.1.2 Test Results and Post-Test Inspection

The tower was subjected to the random vibration test for 60 seconds. Neither observation during the test nor a post-test inspection (including removal of the walls) revealed any sign of damage.

The carbon foam cores did release a very small number of carbon particles (a few tens per stage), confirming the inadequacy of that material for this application. The carbon particles were actually released during assembly of the walls because of small local deformations induced by tightening the screws.

The corner spacers separating the lowest tray from the base plate rotated around their vertical axis by about 45 degrees during the test, indicating a loss of frictional forces due to dynamic loads. These corners were easily rotated back to their original position. Note that an actual flight design would have the corner spacers as part of the trays instead of separate pieces, which would prevent their rotation.

Base to top transfer functions measured before the test, immediately after the test, and then after rotating the corner blocks back in position, are compared in Fig. 45. The data shows that the test led to a small reduction in stiffness, particularly in the fundamental modes. Part of the loss was recovered after rotating the corners back in position.

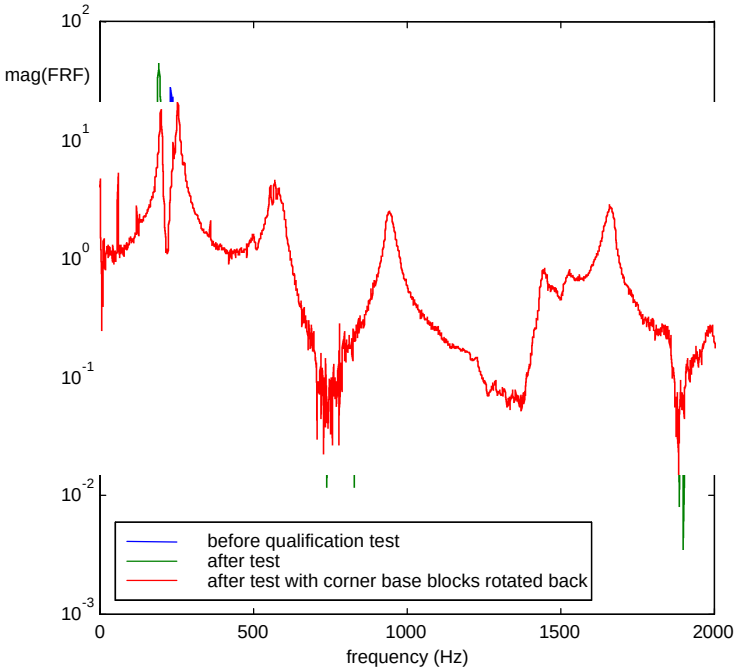

Figure 45: tower with walls; frequency response function from base to top; comparison of pre- and post- test dynamics.

7.3.2 transverse tests without side-walls

Since the tower survived the random vibration tests with side-walls on, we continued with more testing, this time without the side-walls.

7.3.2.1 Notched Vibration Spectrum

The base acceleration PSD is now notched to avoid over-exciting the first 4 lateral modes of the tower without walls. The resulting PSD is shown in Fig. 46 and the actual PSD, measured during the test is compared to the requirement in Fig. 47.

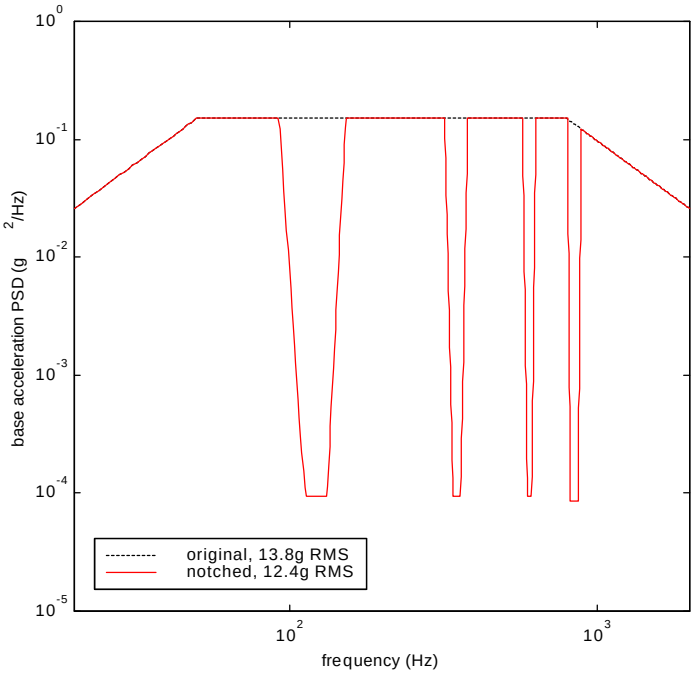

Figure 46: tower without walls; random vibration acceleration PSD notched to avoid excessive excitation of tower bending modes.

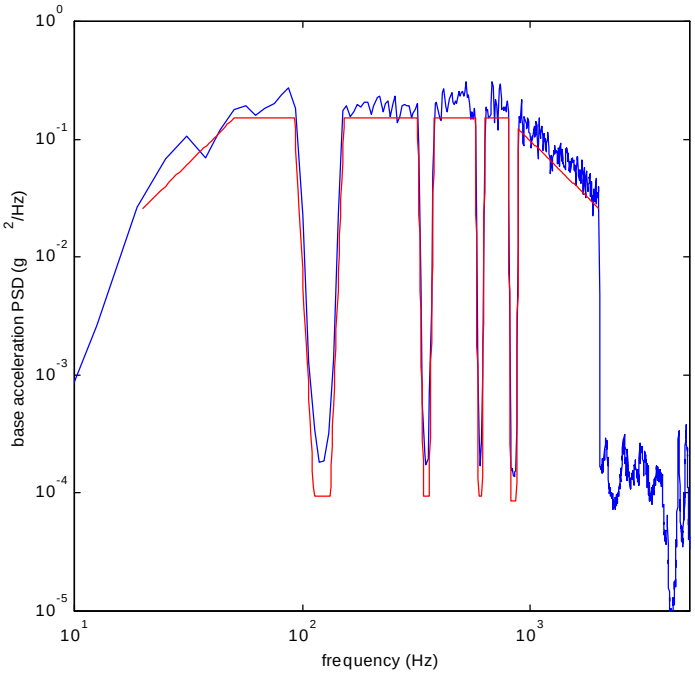

Figure 47: tower without walls; random vibration acceleration PSD notched to avoid excessive excitation of tower bending modes; measured PSD compared to required PSD.

7.3.2.2 Test Results and Post-Test Inspection

The tower was shaken for 60 seconds in one direction, then rotated 90 degrees on the slip table and shaken for another 60 seconds. Close monitoring during the test and a subsequent inspection did not reveal any damage. No further release of carbon particles was observed.

The corner spacer blocks at the lower 3 stages rotated very slightly during the first test (15 degrees at most). Again, this would not occur if the blocks were integral parts of the tray closeout frames. Figure 48 compares measured base-to-top transfer functions before these tests, after the first minute in one direction, and after the second minute in the other direction. No significant difference can be seen, confirming the fact that the tower survived these tests without damage.

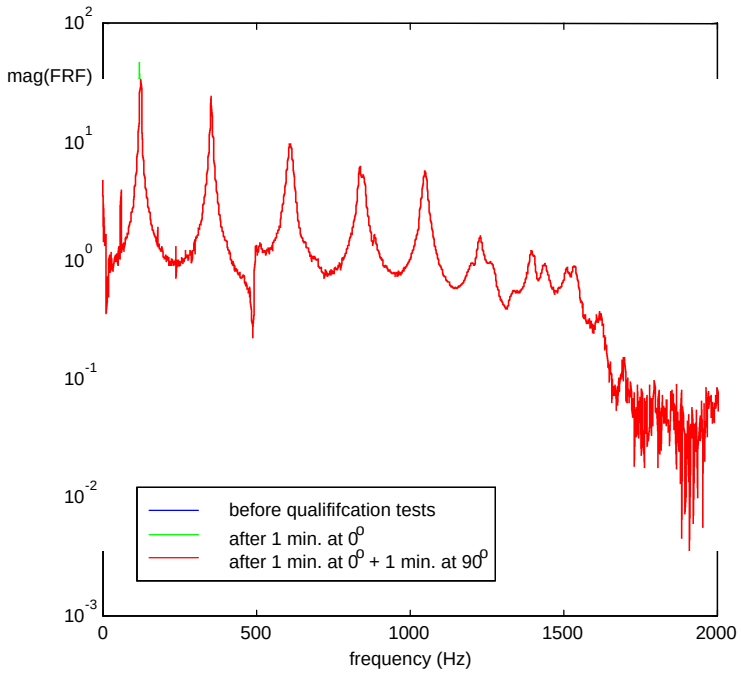

Figure 48: tower without walls; frequency response function from base to top; comparison of pre- and post- test dynamics.

7.3.3 axial test without side-walls

Multiple tests with 60 second exposure each were performed in the launch direction. The base vibration PSD was attenuated through a hypothetical spacecraft (see below) to prevent undue damage to the trays from excessive excitation of the numerous tray drum modes.

7.3.3.1 spacecraft-attenuated vibration spectrum

A hypothetical spacecraft/instrument combination, with a first resonant frequency of 35 Hz in the launch direction was assumed. As explained in the introduction to Section 7.3, the attenuation was assumed to be –20dB/decade above that frequency (1/*f*). The filtering function and the resulting base acceleration PSD used in the test are shown in Fig. 49.

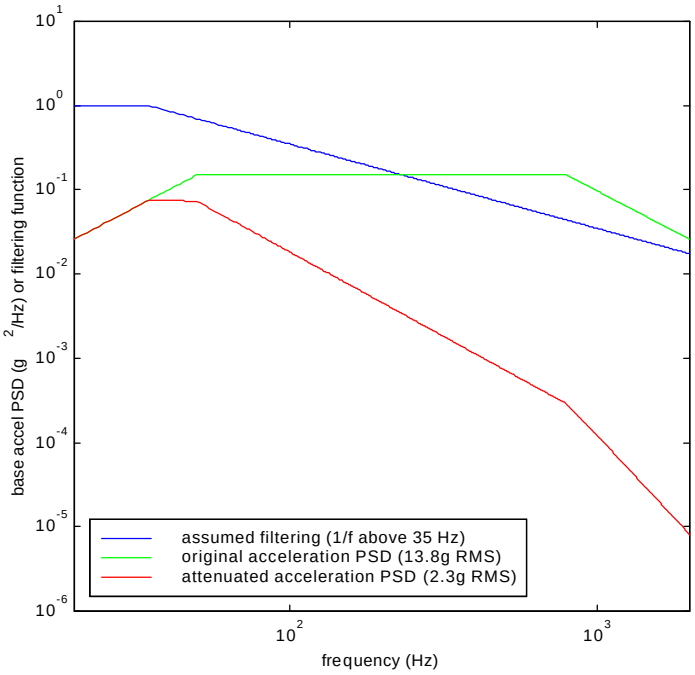

Figure 49: vibration attenuation from hypothetical spacecraft/instrument combination with 35 Hz fundamental frequency and the resulting base acceleration PSD used in the test.

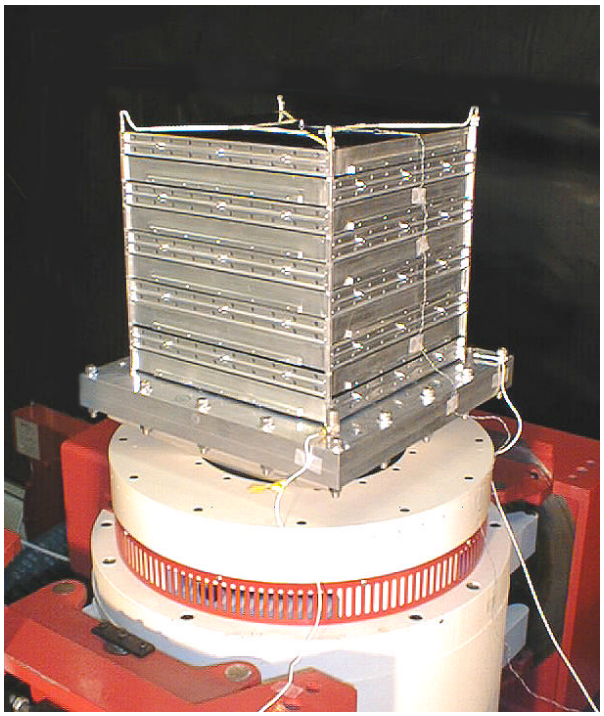

Figure 50: tower undergoing qualification tests in the launch direction.

7.3.3.2 Test Results and Post-Test Inspection

The structure was first subjected to the filtered spectrum of Fig. 49 for 60 seconds. No damage could be detected. Note that the RMS acceleration in the filtered spectrum is reduced to 2.3 *g*RMS, compared to 13.8 *g*RMS in the original, unfiltered PSD. To increase the *g* level and produce a more severe workmanship test, we then amplified the filtered spectrum by a flat, uniform gain of +10dB (factor 10 on PSD), bringing the RMS *g* level up to 7.3 *g*RMS. The tower survived 60 seconds exposure to this increased level without detectable damage. Note that we were not able to amplify the filtered spectrum back up to 13.8 *g*RMS (+15dB) because we were reaching the velocity limits of the shaker (at a given *g* level, the velocity is higher for lower frequencies).

As before, transfer functions from base to top tray were measured before and after those tests. The measurements are compared in Fig. 51 and do not show any change in tower dynamics.

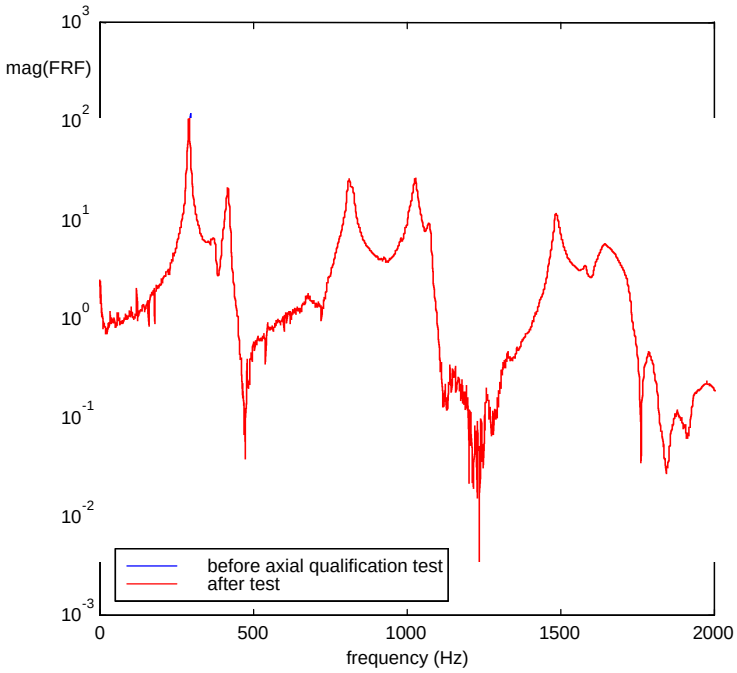

Figure 51: vertical frequency response functions from motion of the base plate to that of the middle of the top tray; comparison of pre- and post-test measurements.

7.4 Assessment of Tray Alignment Accuracy VS Manufacturing Tolerances

At the conclusion of the qualification tests, some rough measurements were performed to evaluate the alignment inaccuracies in the tower. Note that the prototype hardware was not manufactured to tolerances as tight as would be used for flight hardware. However, the data provides insight into relationship between manufacturing tolerances and tray positioning accuracy.

The measurements were performed with dial indicators with a resolution of .0001". Four points on the top of the center rib, near the corners, were measured in the vertical direction to evaluate roll and pitch inaccuracies of each tray (the bottom tray could not be measured for lack of reach). In addition, the relative horizontal positions of the corners of the trays were gaged to

evaluate lateral misalignments. The results show maximum deviations from perfect transverse alignment of about .004" (100 microns); this is consistent with the manufacturing tolerances imposed on the tray closeout. The vertical measurements were processed to extract off-horizontal angles of the trays around the 2 principal axes of the tower. Those results are summarized in Fig. 52 and are again consistent with manufacturing tolerances. The measured angles translate to at most 75 microns on the vertical position differential from one edge of a tray to the other.

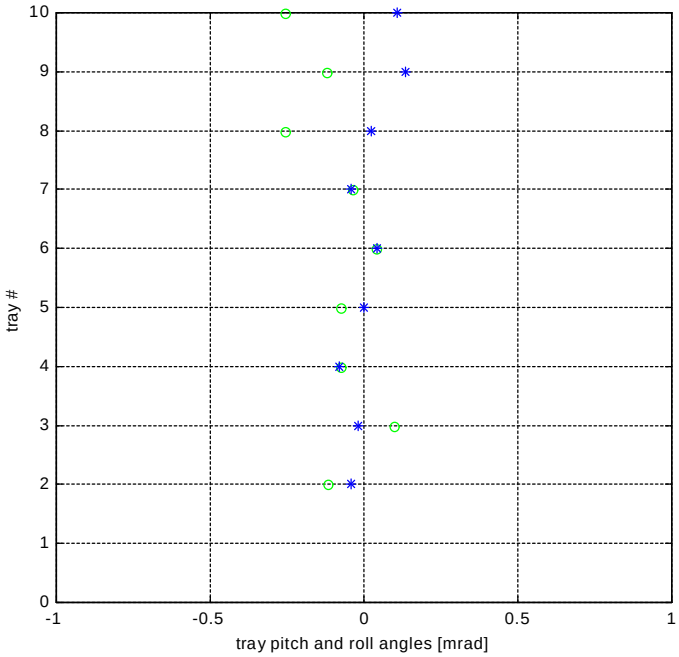

Figure 52: measured roll and pitch angles of 9 of the 10 trays, after qualification tests (form planar least square fit through 4 measured points per tray).

7.5 Tower Disassembly and Final Inspection

At the end of the tests described above, the tower was completely disassembled for a final inspection.

First, the cable tensioning fixture of Fig. 16 was reinstalled on the base plate and used to measure the amount of load remaining in the cables (approximately). The results show between 158 lbf and 163 lbf of residual load, or a 24% apparent relaxation in the cables, over a 15 day period. The relaxation is most likely the result of creep in the Kevlar fibers. The relaxation would be a critical issue for a tower relying exclusively on the corner cables for structural integrity. However, our proposed Phase II design makes use of the side-walls as structural members, providing the largest part of the tower stiffness and strength. With these walls, the cables are only required to provide structural integrity during assembly and testing of the towers, under a 1 *g* environment.

The tower was then disassembled, one layer at a time and the trays, corner spacer blocks, tubular pins, and cables were visually inspected (with 30x magnification in some cases) for signs of damage. The inspection did not reveal any troubling damage. As expected, the contact

surfaces of the corner spacer blocks and the tray closeout frames show minor fretting marks from the high contact pressure and dynamic cycling.

Each tray was also carefully examined after disassembly for the tower; no signs of delaminations of face sheets or debonding or payload components could be found.

8. Phase I Design Evaluation and Conclusions

The most important conclusion of this Phase I is that the concept of stacking trays and relying on corner cables for structural integrity of the resulting tower is a viable one: it can be and was designed to survive severe random vibration tests for space-launched equipment. No damage to the tower components could be detected at the end of those tests. Two minor issues deserve further attention in developing advanced concepts for Phase II. They are the pronounced relaxation of the cable preload over time (although this becomes a much less important issue once side-walls are added to the design), and the minor pitting that occurs from large static pressure at interfaces between trays, combined with substantial dynamic loads. Susceptibility of advanced composites to this type of pitting will be investigated.

The assembly and alignment concept, using tubular centering pins and closely controlled dimensional tolerances on the tray corner pieces effectively produced a tower with small and predictable errors in tray to tray alignment. The tolerances used for the prototype trays were much looser than achievable with modern manufacturing techniques; even then, the assembled tower comes close to satisfying alignment tolerances for the GLAST tracker towers. Fabrication and of structural components did not pause any particular problems; the assembly tooling designed for this project performed as expected, making assembly and checkout of the tower particularly convenient.

A two-level simulation approach was used and validated. Low level, detailed finite element models are used to design and analyze components and assemblies. These models can then effectively be used to adjust simpler lumped parameter dynamic models that can then be used to predict random vibration response and to quickly explore the effects of various design parameters. Comparison of simulation results from those two types of models with experimental measurements on the trays and tower showed excellent agreement, thereby validating this analysis approach for development of advanced designs in Phase II.

Although the corner cables alone were shown to be sufficiently strong to hold towers together, a substantial increase in bending and torsional stiffness of the tower can be achieved by attaching full-coverage side-walls to the tower. Note that, in GLAST, such walls are required anyway to provide a thermal path for conducting waste heat from the tray electronic modules down to the instrument “backbone” (the grid) and from there out to the radiators. Using this approach, stiffness requirements for the trays themselves are lessened and the amount of structural material in the trays can be reduced, potentially leading to a lighter tower. The addition of side –walls introduces new design issues. The attachment of those walls to the side of trays in particular will require attention: whatever attachment method is used, it must provide adequate mechanical coupling of the walls to the tower as well as good thermal transfer properties. Within the limits of available space, a removable attachment is also preferable for maintenance purposes.

Testing has shown that, when using advanced, unusual materials in the design of those structures, it is essential to test samples to evaluate critical thermal and mechanical properties.

Those tests are needed, not only to allow accurate predictions of structural and thermal behavior via analysis, but also as a quality control step. Data obtained from vendors are not always reliable because of variations in manufacturing parameters.

In summary, this Phase I effort has, by designing, analyzing, and testing a full size prototype clearly confirmed the validity of the proposed stacked tray concept for use as support structures for space based particle tracking detectors. The design and analysis methodology used in Phase I have been fully validated by comparison with test data and is ready for full implementation in the development of advanced ultra-lightweight composite material structures in Phase II.

9. References

1. *Mark s Standard Handbook for Mechanical Engineers,* 8th ed., Baumeister *et al.*, ed., McGraw-Hill, pp. 3-26.
2. *Handbook of Composites*, George Lubin, Ed., Van Nostrand Reinhold Co., New York, NY, 1982.
3. Cortland Cable Company, Inc., P.O. Box 330-177, Port Watson St., Cortland, NY 13045.
4. *Designer s Reference Guide to Adhesive Technology*, 3M, Industrial Adhesives and Aerospace Department, Industrial Tape and Specialties Division, 3M Center Bldg. 220-7E-01, St. Paul, MN 55144-1000, 1995.
5. Cytec Engineered Materials, Inc., Anaheim, CA 92806, 1-800-647-3746.
6. Data Physics Corporation, 2085 Hamilton Ave., Ste 200, San Jose, CA 95125, www.dataphysics.com.
7. DSP Technology, Inc., Signal Analysis Group, 48500 Kato Rd., Fremont, CA 94538-7385.
8. Matlab Software, The MathWorks, Inc., 24 Prime Park Way, Natick, MA 017060, http://www.mathworks.com.
9. *Structural Dynamics Toolbox* for Matlab, E. Balmes, Ed., Scientific Software Group, http://www.ssg.fr/sdt, 20 rue Troyon, 92136 Sevres, France, 1997.
10. Pacific Testing Laboratories, Inc., 24950 Avenue Tibbetts, Valencia, CA 91355.
11. YLA Composites, Inc., 2970 Bay Vista Court, Benicia, CA 94510.
12. M. F. Ashby, "The Mechanical Properties of Cellular Solids," *Metallurgical Transactions A*, Vol. 14a, pp. 1755-1769, Sept. 1983.
13. Energy Research and Generation, Inc., 900 Stanford Ave., Oakland, CA 94608.
14. *Shock and Vibration Handbook*, 3rd Edition, C. M. Harris, Ed., McGraw-Hill, 1988.
15. *General Environmental Verification Specification for STS & ELV Payload, Subsystems, and Components*, GEVS-SE Rev. A, System Reliability and Safety Office, Code 302, NASA/Goddard Space Flight Center, Greenbelt, MD 20771-0001, June 1996.

REPORT DOCUMENTATION PAGE

Form Approved
OMB No. 0704-0188

1. AGENCY USE ONLY *(Leave blank)*	2. REPORT DATE	3. REPORT TYPE AND DATES COVERED
	October 7, 1998	SBIR Phase I, Final, April 10 to October 9, 1998

4. TITLE AND SUBTITLE
Innovative, Low-Mass, Passively Cooled, All Composite Material Tower Structure for High Resolution Charged Particle Tracking in a Gamma-Ray Space Telescope

5. FUNDING NUMBERS
C NAS5-98102

6. AUTHORS
Eric R. Ponslet, Steven A. Ney, and William O. Miller

7. PERFORMING ORGANIZATION NAME(S) AND ADDRESS(ES)
HYTEC Inc.
110 Eastgate Drive
Los Alamos, NM 87544

8. PERFORMING ORGANIZATION REPORT NUMBER
HYTEC-TN-NASASBIR-03

9. SPONSORING/MONITORING AGENCY NAME(S) AND ADDRESS(ES)
NASA Goddard Space Flight Center
Engineering Procurement Office
Greenbelt, MD 20771

10. SPONSORING/MONITORING AGENCY REPORT NUMBER

11. SUPPLEMENTARY NOTES

12a. DISTRIBUTION/AVAILABILITY STATEMENT

12b. DISTRIBUTION CODE

13. ABSTRACT *(Maximum 200 words)*

Our objective is the development of ultra-lightweight support structures for high precision space based instruments. The structures must provide efficient passive cooling and survive severe vibrations during launch. HYTEC has introduced an innovative concept of stacked tray structures with synthetic cable restraints that could lead to substantial improvements for future experiments such as GLAST.

The objectives of Phase I were to demonstrate the feasibility of the stacked tray concept, to validate design and analysis approaches for this concept, and experimentally evaluate a prototype assembly for its ability to survive random vibrations during launch. During the Phase I period, a complete prototype of the stacked tray concept was built and tested at HYTEC. Numerical simulations were performed to predict dynamic response of the structure. Those predictions were compared to experimental data from a series of modal tests performed on the prototype. Analytical-experimental agreement was very good. Finally, the prototype was subjected to random vibration qualification tests and survived without damage.

The report details the mechanical design of the prototype, its fabrication and assembly, and structural testing. Simulation techniques and results are detailed and compared to measurements. Random vibration qualification tests are described. Lessons learned and plans for Phase II are included.

14. SUBJECT TERMS
ultra-lightweight structural design, space based instruments, stacked tray, silicon strip detectors, Kevlar cables, analytical structural dynamics, experimental structural dynamics, lumped parameter simulation, random vibration, qualification test

15. NUMBER OF PAGES
55

16. PRICE CODE

17. SECURITY CLASSIFICATION OF REPORT	18. SECURITY CLASSIFICATION OF THIS PAGE	19. SECURITY CLASSIFICATION OF ABSTRACT	20. LIMITATION OF ABSTRACT